Author Manuscript

Author Manuscript

Author Manuscript

Author Manuscript

HHS Public Access

Author manuscript

Nature. Author manuscript; available in PMC 2025 January 10.

Published in final edited form as:

Nature. 2024 July ; 631(8022): 857–866. doi:10.1038/s41586-024-07627-2.

Interferon subverts an AHR-JUN axis to promote CXCL13+ T cells in lupus

Calvin Law[1,2,3,*], **Vanessa Sue Wacleche**[4,*], **Ye Cao**[4,*], **Arundhati Pillai**[1,2,3], **John Sowerby**[4], **Brandon Hancock**[1,2,3], **Alice Horisberger**[4], **Sabrina Bracero**[4], **Viktoriya Skidanova**[4], **Zhihan Li**[4], **Ifeoluwakiisi Adejoorin**[4], **Eilish Dillon**[4], **Isaac J. Benque**[4], **Diana Pena Nunez**[4], **Daimon P. Simmons**[4,5], **Joshua Keegan**[6], **Lin Chen**[4], **Tina Baker**[7], **Phillip Z. Brohawn**[7], **Hussein Al-Mossawi**[8], **Ling-Yang Hao**[9], **Brian Jones**[9], **Navin Rao**[9], **Yujie Qu**[10], **Stephen E. Alves**[10], **Accelerating Medicines Partnership: RA/SLE Network**, **A. Helena Jonsson**[4], **Katharina S. Shaw**[11], **Ruth Ann Vleugels**[11], **Elena Massarotti**[4], **Karen H. Costenbader**[4], **Michael B. Brenner**[4], **James A. Lederer**[5], **Judd F. Hultquist**[12], **Jaehyuk Choi**[1,2,3,13,14,#], **Deepak A. Rao**[4,#]

[1]Department of Biochemistry and Molecular Genetics, The Feinberg School of Medicine, Northwestern University, Chicago, IL, USA

[2]Department of Dermatology, The Feinberg School of Medicine, Northwestern University, Chicago, IL, USA

[3]Center of Human Immunobiology, The Feinberg School of Medicine, Northwestern University, Chicago, IL, USA

[4]Division of Rheumatology, Inflammation, and Immunity, Brigham and Women's Hospital and Harvard Medical School, Boston, Massachusetts, USA

[5]Department of Pathology, Brigham and Women's Hospital, Boston, Massachusetts, USA

Deepak A. Rao, Hale Building for Transformative Medicine, Room 6002R, 60 Fenwood Road, Boston MA 02115, darao@bwh.harvard.edu, Jaehyuk Choi, Robert H Lurie Medical Research Center, Room 5-115, 303 E Superior St, Chicago IL 60611, jaehyuk.choi@northwestern.edu.

*These authors contributed equally

#These authors jointly supervised the work

Author contributions

C.L. and V.S.W. designed and performed experiments, analyzed data and wrote the manuscript; Y.C. performed computational analysis and wrote the manuscript. C.L. organized CRISPR screen libraries and performed CRISPR arrayed screens. C.L performed ELISA assays for the CRISPR screens with the assistance from A.P., B.H., and V.S.W.. C.L. performed CUT&RUN assays, T cell functional assays, time course RNA-seq assay, computational analyses, and organizing and designing of figures for manuscript. A.P performed co-immunoprecipitation assays. V.S.W. performed T cell functional and phenotyping analyses with assistance from V.S, I.A., I.B., and D.P.N.. Y.C. and C.L. performed bulk RNA-seq and D.S. participated in bulk RNA-Seq analyses. V.S. performed luciferase assays. T.B., P.Z.B., and H.A-M. provided and analyzed anifrolumab clinical trial data. J.K., S.E.A., Y.Q., and J.A.L. generated mass cytometry data, and A.H. analyzed mass cytometry data. S.B. generated and analyzed in vitro scRNA-Seq data, and A.H., J.S., L-Y.H., B.J., and N.R. participated in analysis of these data. M.B.B. and A.H.J. contributed to generation and analysis of AMP T cell scRNA-Seq analysis. K.H.C., E.M., R.A.V, K.S.S, E.D., A.H., and L.C. participated in evaluation of SLE patient clinical data. J.F.H. contributed to design and execution of CRISPR array experiments. D.A.R. and J.C. conceived and supervised the study, analyzed and interpreted data and wrote the manuscript. All authors contributed to editing the manuscript.

Declaration of interests

The work was performed in part with grant support from Merck Sharpe & Dohme and from Janssen Research & Development, LLC. D.A.R. reports personal fees from Pfizer, Janssen, Merck, GlaxoSmithKline, AstraZeneca, Scipher Medicine, HiFiBio, and Bristol-Myers Squibb, and grant support from Bristol-Myers Squibb and Merck outside the submitted work. D.A.R. and M.B.B. are co-inventors on a patent on Tph cells as a biomarker of autoimmunity. T.B. and P.Z.B. are employees of AstraZeneca. H.A.-M. was an employee of AstraZeneca during the study period. L.-Y.H., B.J., and N.R. are employees of Janssen Research & Development, LLC. S.E.A. and Y.Q. are employees of Merck & Co., Inc.. A patent application has been submitted based on this work.

Author Manuscript Author Manuscript Author Manuscript Author Manuscript

[6]Department of Surgery, Brigham and Women's Hospital, Boston, Massachusetts, USA

[7]AstraZeneca, Gaithersburg, MD

[8]AstraZeneca, Late Respiratory and Immunology, Cambridge, UK

[9]Discovery Immunology, Janssen Research & Development, Spring House, PA

[10]Merck & Co., Inc., Rahway, NJ, USA

[11]Department of Dermatology, Brigham and Women's Hospital, Boston, Massachusetts, USA

[12]Division of Infectious Diseases, The Feinberg School of Medicine, Northwestern University, Chicago, IL, USA

[13]Center of Synthetic Biology, Northwestern University, Chicago, IL, USA

[14]Center for Genetic Medicine, Northwestern University, Chicago, IL, USA

Summary paragraph

SLE is prototypical autoimmune disease driven by pathologic T cell-B cell interactions[1,2]. Expansion of B cell-helper T cells including T follicular helper (Tfh) and T peripheral helper (Tph) cells is a prominent feature of systemic lupus erythematosus (SLE)[3,4]. Human Tfh and Tph cells characteristically produce high levels of the B cell chemoattractant CXCL13[5,6], yet regulation of T cell CXCL13 production and the relationship between $CXCL13^+$ T cells and other T cell states remains unclear. Here, we identify an imbalance in CD4 T cell phenotypes in SLE patients, with expansion of $PD\text{-}1^+/ICOS^+$ $CXCL13^+$ T cells and reduction of $CD96^{hi}$ $IL\text{-}22^+$ T cells. Using CRISPR screens, we identify the aryl hydrocarbon receptor (AHR) as a potent negative regulator of CXCL13 production by human CD4 T cells. Transcriptomic, epigenetic, and functional studies demonstrate that AHR coordinates with AP-1 family member JUN to prevent $CXCL13^+$ Tph/Tfh cell differentiation and promote an $IL\text{-}22^+$ phenotype. Type I interferon (IFN), a pathogenic driver of SLE[7], opposes AHR and JUN to promote T cell production of CXCL13. These results place $CXCL13^+$ Tph/Tfh cells on a polarization axis opposite from Th22 cells and reveal AHR, JUN, and IFN as key regulators of these divergent T cell states.

Keywords

T peripheral helper; T follicular helper; CXCL13; systemic lupus erythematosus; aryl hydrocarbon receptor; JUN; AP-1; interferon

---

Both activated B cells and B cell-helper T cells are expanded in patients with SLE and correlate with disease activity[3,4,8–10]. Chronic autoimmune diseases such as SLE often involve expansion of a range of B cell-helper T cells including Tfh cells, which help B cells within lymphoid follicles[11], and Tph cells, which help B cells within inflamed peripheral tissues[3,6]. In addition to production of IL-21 and CD40L, a hallmark function of human B cell-helper T cells is the secretion of CXCL13, a B cell chemoattractant that uniquely binds CXCR5[12]. The extrinsic signals and transcriptional networks that control CXCL13 production by T cells remain largely unknown, with roles for TGF-β, IL-2, and SOX4

Author Manuscript Author Manuscript Author Manuscript Author Manuscript

previously reported[13,14]. Further, how CXCL13$^+$ Tph and Tfh phenotypes fit in the context of other differentiated T cell states remains unclear.

Skewed Tph/Tfh versus Th22 cells in SLE

To broadly evaluate alterations in CD4$^+$ T cells in SLE, we used mass cytometry to compare blood CD4$^+$ T cells from 19 patients with SLE and 19 non-autoimmune controls (Supplementary Table 1). Differential expression analyses identified increased expression of PD-1, KI67, and TBET in T cells from SLE patients and increased expression of CD96 in cells from controls (Extended Data Fig. 1a; Supplementary Table 2). Differential abundance analyses using co-varying neighborhood analysis (**CNA**)[15] visualized by uniform manifold approximation and projection (**UMAP**) indicated an enrichment in neighborhoods containing PD-1/ICOS$^+$ cells in SLE patients, while distinct neighborhoods containing CD96^{hi} cells were enriched in controls (Fig. 1a,b). Differential abundance analysis of cell clusters confirmed enrichment of PD-1/ICOS+ cells and depletion of CD96^{hi} cells in SLE patients (PD-1/ICOS+ cells, cluster 8, OR=2.8, p=0.0002; CD96^{hi} cells, cluster 7, OR=0.3, p=3.13e-09) (Fig. 1c,d, Extended Data Fig. 1b). The abundance of the PD-1$^+$/ICOS$^+$ cluster was inversely correlated with the CD96^{hi} cluster and was positively associated with disease activity level and anti-double stranded DNA antibody level but not with immunosuppressive drug treatment (Extended Data Fig. 1c–g).

We performed bulk RNA-Seq to interrogate the potential functions of the highlighted T cell subsets (Extended Data Fig. 2a,b). Both PD-1^{hi} CXCR5$^-$ and PD-1^{hi} CXCR5$^+$ populations expressed genes characteristic of Tph/Tfh cells including *MAF, CXCL13,* and *PDCD1* (Fig. 1e,f), as previously described[3]. In contrast, CD96^{hi} cells selectively expressed *IL22*, *CCR6, RORC,* and *AHR,* but not *IL17A* or *IL17F*, indicative of Th22 cells. Th22 cells share features with Th17 cells but are distinguished by lower production of IL-17A and higher production of IL-22[16], a cytokine that promotes epithelial barrier integrity and wound healing[17] (Fig. 1e, Extended Data Fig. 2e, Supplementary Table 3). CD96^{hi} cells showed the highest enrichment score for a Th22-associated gene set (Fig. 1f). Analysis of T cell subsets from PBMC of additional SLE patients confirmed increased *IL22* in CD96^{hi} T cells and higher *CXCL13* in Tfh and Tph cells (Extended Data Fig. 2d).

In vitro stimulation confirmed that CD96^{hi} cells from healthy donors frequently produced IL-22 protein, often without co-production of IL-17A (Fig. 1g, Extended Data Fig. 2e). CD96^{hi} cells produced IFN-γ and TNF comparably to Tfh/Tph cells but more frequently expressed CCR6, a receptor expressed by Th17 and Th22 cells (Extended Data Fig. 2f,g). Thus, SLE patients show a marked expansion of CXCL13$^+$ Tfh/Tph cells and a concurrent reduction in IL-22-producing CD96^{hi} T cells.

AHR inhibits CXCL13+ Tph differentiation

The imbalance in CXCL13$^+$ versus IL-22$^+$ T cells in SLE patients suggested that CXCL13 and IL-22 may exist on opposite sides of an axis of T cell differentiation. To identify molecular drivers of these distinct phenotypes, we performed an arrayed CRISPR depletion screen in memory CD4$^+$ T cells, targeting 86 candidate genes and 10 control

Author Manuscript Author Manuscript Author Manuscript Author Manuscript

genes with CRISPR-Cas9 ribonucleoproteins (crRNPs), to identify regulators of CXCL13 production. These 86 target genes were selected from genes upregulated in Tph/Tfh cells (Supplementary Table 4) or correlated with CXCL13 expression[13,14].

Memory CD4$^+$ T cells from 2 healthy donors were nucleofected with the arrayed crRNP libraries and cultured for 4 days in the presence or absence of TGF-β, an inducer of CXCL13 production[13] (Fig. 2a. Deletion of *CD3* or *LCP2* (also called *SLP-76*), two proteins critical for TCR signaling included as positive controls, inhibited CXCL13 production (Fig. 2b, Extended Data Fig. 3a). Cbl Proto-Oncogene B (*CBLB*), an E3 ubiquitin ligase, and the aryl hydrocarbon receptor (*AHR*) were the top regulators of CXCL13 production; deletion of either gene strongly upregulated CXCL13 production in the absence or presence of TGF-β (Fig. 2b, Extended Data Fig. 3b).

We focused on AHR because of its recognized role in promoting IL-22 production and Th22 differentiation[16,18,19]. CRISPR deletion of AHR in multiple donors confirmed that AHR deletion increases CXCL13 production (Extended Data Fig. 3c,d), which was further enhanced by TGF-β (Extended Data Fig. 3e). In parallel, deletion of AHR decreased production of IL-22 (Extended Data Fig. 3d). Similarly, the AHR inhibitor CH-223191 (AHRinh) increased CXCL13 and decreased IL-22 production, with similar effects in naïve and memory CD4$^+$ cells (Fig. 2c, Extended Data Fig. 3f,g). In contrast, AHR agonist 2,3,7,8-tetrachlorodibenzodioxin (TCDD) decreased CXCL13 production and increased IL-22 production. Similar results were obtained with a second AHR agonist, 6-formylindolo(3,2-b)carbazole (FICZ), and a second AHR inhibitor, GNF-351 (Extended Data Fig. 3h). Neither CRISPR deletion nor pharmacological modulation of AHR substantially affected IFN-γ production (Extended Data Fig. 3i). Further, AHR agonism did not suppress *in vitro* polarization of CD4 T cells into IFN-γ$^+$ Th1 cells, IL-4$^+$ Th2 cells, or IL-17A$^+$ Th17 cells, indicating that AHR selectively suppresses CXCL13 production (Extended Data Fig. 3j).

Among several factors associated with Tfh or Th17/Th22 differentiation, only TGF-β and modulation of AHR activity altered CXCL13 and IL-22 production (Extended Data Fig. 3k). AHR inhibition also increased ICOS expression and decreased CD96 expression on CD4$^+$ T cells, while AHR activation had opposite effects (Fig. 2d). Both CRISPR deletion and pharmacologic inhibition of AHR had similar effects on CD8$^+$ T cells, with increased CXCL13 and ICOS but decreased IL-22 and CD96. Conversely, AHR activation in CD8+ T cells decreased CXCL13 and increased IL-22 (Extended Data Fig. 3l–n). Together, these data suggest that CXCL13 production and IL-22 production lie on opposites ends of a T cell differentiation axis that is regulated by AHR and TGF-β.

To determine the effects of AHR activity on CXCL13 and IL-22 in the setting of persistent TCR activation, memory and naïve CD4$^+$ T cells were stimulated weekly for 3 weeks in the presence or absence of AHR modulators. Repeated stimulation induced progressively higher production of CXCL13 over time, while production of IL-22 and IFN-γ remained stable (Extended Data Fig. 4a). CXCL13 production was amplified by the AHR inhibitor, while AHR agonism blunted the rise in CXCL13 production over time.

Author Manuscript Author Manuscript Author Manuscript Author Manuscript

TGF-β and AHR control Tph features

To determine broader transcriptomic changes associated with the CXCL13^{+} phenotype induced by TGF-β and AHR inhibition, we performed a single cell RNA-Seq (**scRNA-Seq**) analysis of memory CD4^{+} T cells from 3 donors after 2 weeks of culture with DMSO, TGF-β+DMSO, TGF-β+AHR agonist (TCDD), or TGF-β+AHR inhibitor (CH-223191). By UMAP visualization, cells treated with TGF-β or TGF-β+AHR inhibitor were spatially separated from cells not treated with TGF-β (Fig. 2e). Cells treated with TGF-β+AHR agonist clustered together with cells not treated with TGF-β, suggesting that AHR agonism inhibited the transcriptomic program induced by TGF-β. T cells cultured with TGF-β+AHR inhibitor or TGF-β+DMSO co-localized in a specific region of the UMAP that demonstrated the highest expression of a Tph gene signature (Fig. 2f). We then compared these *in vitro* differentiated cells to a reference map of T cells from RA synovium[20] (Extended Data Fig. 4b, Supplementary Table 5). T cells treated with TGF-β+AHR inhibitor or TGF-β+DMSO preferentially mapped to the synovial Tph cell cluster (cluster 9), while DMSO-treated cells and TGF-β+AHR agonist-treated cells preferentially mapped to a distinct region (cluster 3) (Extended Data Fig. 4c,d).

Bulk RNA-Seq analyses similarly showed that CD4^{+} T cells stimulated with TGF-β+AHR inhibitor upregulated CXCL13 and a Tph signature compared to TGF-β+TCDD-treated cells (Extended Data Fig. 4e,f). Comparison of T cell transcriptomes from the strongest CXCL13-inducing condition (TGF-β+AHR inhibitors for 2 weeks) versus the weakest CXCL13-inducing condition (TCDD only for 1week) showed a significant enrichment of Tph-associated genes in the TGF-β+AHR inhibitor condition and an enrichment for CD96^{hi}-associated genes in the AHR agonist condition (Fig. 2g). TGF-β alone induced a Tph signature when AHR was inhibited yet could not induce a Tph signature when AHR was activated (Extended Data Fig. 4g).

We confirmed a strong interaction between TGF-β and AHR at the protein level across diverse T cell subsets. In the presence of TGF-β, both CRISPR deletion of AHR and AHR inhibition induced CXCL13 production from multiple sorted T cell subsets, including Tph cells, Tfh cells, Th17 cells, and Th1 cells (Extended Data Fig. 5a,b). The ability of AHR inhibition to induce CXCL13 production depended on the presence of TGF-β for most cell subsets; however, Tph cells showed a unique ability to produce CXCL13 with AHR inhibition alone without co-treatment with TGF-β. Tph cells from SLE patients showed higher expression of a TGF-β response gene signature, suggesting recent exposure to TGF-β *in vivo*, obviating the need for exogenous TGF-β (Extended Data Fig. 5c). Both TGF-β and AHR inhibition reduced IL-22 production from CD96^{hi} and Th17 cells, yet AHR activation did not induce IL-22 production from Tph or Tfh cells (Extended Data Fig. 5d). AHR inhibition also increased ICOS and PD-1 expression in stimulated Tph, Tfh, CD96^{hi}, and naïve cell subsets while suppressing CD96 and TIGIT expression (Extended Data Fig. 5e).

Next, we used ATAC-Seq to evaluate the extent to which AHR inhibition induces epigenetic features of Tph and Tfh cells. We generated ATAC-Seq profiles of PD-1^{hi} CXCR5^{-} Tph cells from RA synovial fluid (**SF**) and PD-1^{hi} CXCR5^{+} Tfh cells from tonsil and used DESeq2[21] to identify differentially accessible regions (**DAR**) in Tph and Tfh cells by

Author Manuscript Author Manuscript Author Manuscript Author Manuscript

comparing them to PD-1^{lo} cells from the same tissue (Extended Data Fig. 6a–d). We then compared these regions to DAR found in CD4 T cells stimulated *in vitro* with TGF-β+TCDD or TGF-β+AHR inhibitor. We found that DAR annotated genes of CD4$^+$ T cells treated with TGF-β+AHR inhibitor were significantly enriched for both Tph- and Tfh-associated DAR annotated genes (p=0.001 for both), including opening at the *CXCL13* locus (Extended Data Fig. 6e,f).

We hypothesized that aberrant AHR activation may be a systemic feature in SLE patients that allows for expansion of Tph and Tfh cells. We tested the effects of serum from SLE patients on a HepG2 cell line with a luciferase reporter driven by AHR response elements[22]. Treatment of HepG2 reporter cells with serum from SLE patients significantly inhibited TCDD-induced activation of the AHR reporter, as compared to serum samples from anti-nuclear antibody$^+$ (ANA$^+$) control patients (Fig. 2h. We then tested whether strong AHR activation *in vitro* was sufficient to reduce the frequency of PD-1$^+$ Tph or Tfh cells within PBMC from SLE patients. Treatment of PBMC from SLE patients with the AHR agonist significantly reduced the frequency of PD-1$^+$ CXCR5$^-$ cells among memory CD4$^+$ T cells (Fig. 2i, Extended Data Fig. 7). In addition, pre-treatment of blood PD-1^{hi} CXCR5$^+$ Tfh cells from control donors with TCDD reduced the ability of Tfh cells to induce B cell differentiation into plasmablasts *in vitro* (Fig. 2j).

JUN mediates CXCL13-IL22 polarization

To capture early transcriptional events induced by AHR agonism, we performed a high-resolution time-course RNA-Seq of CD4$^+$ memory T cells treated with TGF-β and either an AHR agonist or inhibitor (Extended Data Fig. 8a). Expression of canonical AHR target genes (*CYP1B1*, *TIPARP*, *AHRR*)[23–25] increased within 12 hours of culture with TCDD. Principal component analysis (PCA) analysis revealed clear separation of samples based on AHR activation status (Extended Data Fig. 8b–e, Supplementary Table 6). AHR agonism significantly enriched AHR target genes and *CD96* expression and downregulated expression of *CXCL13* and other Tph/Tfh genes such as *ICOS*, *MAF* and *IL21* at 48 hours (Extended Data Fig. 8d, Supplementary Table 6). Pathway analyses identified a statistically significant co-enrichment of AP-1 family transcription factor motifs in putative AHR-upregulated genes. Gene expression pattern clustering with MaSigPro identified one gene set progressively upregulated by AHR activation (cluster 6, Supplementary Table 7, Fig 3a). Genes in cluster 6 were enriched for AHR binding near their promoters (Fig 3b, adjusted p=0.00009) and enriched for AP-1 binding motifs (adjusted p=1.03e-8), with AP-1-AHR co-enrichment observed as early as 12 hours after activation (Extended Data Fig. 8f).

To identify the sites directly bound by AHR, we performed CUT&RUN both on AHR-intact control T cells and on T cells in which AHR was depleted by CRISPR, obtaining 2,736 and 1,379 peaks respectively, with significant enrichment of AHR motifs among differentially bound peaks (Diffbind) in AHR-intact cells (Extended Data Fig. 8g,h). We found specific AHR binding at canonical AHR target genes such as *CYP1B1* and *AHRR*, as well as at enhancers/promoters in *CD96* and *IL22* (Extended Data Fig. 8i, j). AHR also bound to *CXCL13*, *ICOS* and *MAF* gene loci, suggesting direct repression of genes associated

Author Manuscript Author Manuscript Author Manuscript Author Manuscript

with Tph/Tfh cells. A gene set of 210 Th22 signature genes was highly enriched among AHR-bound peaks (Extended Data Fig. 8k, hypergeometric score p=0.0019). Pathway analysis utilizing the Kyoto Encyclopedia of Genes and Genomes (KEGG) database for T cell-specific pathways showed that AHR peak-associated genes were enriched in a Th17 signature (Extended Data Fig. 8l); however, there were no AHR peaks in the *IL17A* or *IL17F* gene loci, consistent with a Th22 phenotype (Supplementary Table 8). Unbiased analysis for transcription factor binding sites in AHR peaks using HOMER revealed enrichment of the expected AHR binding motif (p=1e-37, third most significant motif), as well as multiple motifs shared by the AP-1 transcription factor family (TGA[C/G]TCA) (Fig. 3c, Extended Data Fig. 8h). Thus, both RNA-Seq and AHR CUT&RUN transcription factor motif analyses strongly suggested that AP-1 transcription factors and AHR co-regulate gene expression.

To determine which AP-1 family members regulate CXCL13 versus IL-22 associated phenotypes, we performed an arrayed CRISPR screen targeting 22 AP-1 family members in human memory $CD4^+$ T cells (Supplementary Table 9). Deletion of *JUN* strongly upregulated CXCL13 and downregulated IL-22 production (Fig. 3d–f, Extended Data Fig. 9a–c). RNA-Seq analysis of JUN-deleted cells and JUN-intact cells by GSEA showed significant enrichment of Tph signatures in JUN-deleted cells stimulated with TCDD (FDR<0.001), and also a trend towards depletion of Th22 gene signatures (Fig. 3g).

CUT&RUN analysis of JUN in TCDD-treated memory CD4 T cells identified 6901 peaks, which were significantly enriched for AP-1 sites and for both Th17-associated genes and AHR-associated pathways by EnrichR analysis (Extended Data Fig. 9d). Genome-wide, JUN bound 66% of AHR binding sites, a proportion significantly higher than expected by chance alone (hypergeometric p=1.22e-254, Extended Data Fig. 9e. Notably, both AHR and JUN bound to the same enhancer region of the *IL22* gene locus, while JUN also bound to the promoter (Fig. 3h). Like AHR, JUN also bound to the *CXCL13* gene locus (Fig. 3h). In total, genes associated with peaks bound by both JUN and AHR (989 genes from 1170 peaks, Supplementary Table 10) included 23 genes from the AHR-agonized gene cluster identified by time course RNA-Seq, which was unlikely to occur by chance alone (cluster 6, Fig. 3a, hypergeometric p=2.36e-13, Fig. 3i). Co-immunoprecipitation (coIP) using either HA-tagged AHR (HA-AHR) or Flag-tagged JUN (JUN-Flag) confirmed a biochemical interaction between AHR and JUN (Extended Data Fig. 9f,g). Addition of an AHR agonist or inhibitor had no effect on this protein-protein binding; however, AHR agonism increased JUN abundance in the nucleus (Extended Data Fig. 9h).

We next evaluated the effects of AHR activation or inhibition on JUN binding to target loci (Fig. 3j). AHR inhibition reduced the peak sizes at genes co-bound by AHR and JUN, including at *CXCL13* and *IL22* loci (Fig. 3j). Diffbind analysis confirmed a significant reduction of JUN binding to *IL22* in AHR inhibited conditions (FDR=5.4e-4). AHR inhibition also had broader effects on JUN binding peaks, with 60% of all JUN peaks lost in AHR inhibitor-treated cells, including 87% of peaks not co-bound by AHR (Fig. 3k), suggesting that AHR inhibitors may disrupt overall JUN expression or function. Accordingly, AHR inhibition moderately but significantly reduced levels of total JUN and phospho-S73 JUN in $CD4^+$ T cells (Fig. 3l,m).

Author Manuscript Author Manuscript Author Manuscript Author Manuscript

We hypothesized that restoring JUN levels would rescue IL-22 expression and CXCL13 inhibition. Lentiviral overexpression of JUN (JUN OE) significantly decreased CXCL13 production and increased IL-22 expression, even in cells treated with AHR inhibitor (Fig. 3n, Extended Data Fig. 9i). CUT&RUN analysis showed that JUN overexpression restored DNA binding at *CXCL13* and *IL22* gene loci at regions suppressed by AHR inhibition (Fig. 3o, Extended Data Fig. 9j,k). JUN overexpression also restored JUN binding to other Th17/Th22-associated peaks that are otherwise lost in AHR inhibitor-treated cells (Fig. 3p). RNA-Seq analysis of JUN-overexpressing $CD4^+$ T cells demonstrated enrichment of Th22 signatures and suppression of Tph signatures compared to control cells (Fig. 3q). Collectively, these results suggest that JUN upregulates *IL22* and Th22 genes and inhibits *CXCL13* directly.

Type I IFN induces CXCL13$^+$ Tph cells

We next sought to identify extrinsic factors that may skew the Tph/Tfh versus Th22 axis polarization in SLE patients, and we focused on IFN as a hallmark feature of SLE[26]. T cell subsets from SLE patients displayed prominent upregulation of IFN-stimulated genes (ISGs) (Extended Data Fig. 10a). Using a published RNA-seq dataset[27], we found that CXCL13 expression was higher in T cells from ISG^{hi} SLE patients compared to ISG^{low} patients (Fig. 4a). We then evaluated the effect of blockade of the IFN-α/β receptor (IFNAR) on circulating CXCL13 levels in SLE patients treated with either anifrolumab (anti-IFNAR) or placebo in the TULIP-1 randomized controlled trial[28]. ISG^{hi} patients had significantly higher levels of circulating CXCL13 than ISG^{low} (Fig. 4b). In ISG^{hi} SLE patients, IFNAR blockade with anifrolumab significantly reduced serum CXCL13 levels compared to placebo (p=2.67e-07, linear mixed model [LMM]), while CXCL13 levels remained low and unchanged in ISG^{low} patients (p=0.18).

To evaluate whether IFN promotes Tph cells in SLE patients, we performed scRNA-Seq on $CD3^+$ T cells from blood of patients with lupus (n=7 total; 5 SLE, 2 cutaneous lupus, Supplementary Table 1) obtained before and 1–2 months after treatment with anifrolumab (Fig. 4c,d). Clustering of memory $CD4^+$ T cells identified a Tph cluster (cluster 0), which was enriched for a Tph signature (p<2.2e-16, LMM), and a Th22 cluster (cluster 11), which was enriched for both Th22 and $CD96^{hi}$ gene signatures (p<2.2e-16, linear mixed model, Fig. 4e). An ISG signature was higher in the Tph cluster compared to the Th22 cluster (p=4.57e-8, linear mixed model, Fig. 4f). The Tph cluster had a lower signature of JUN target genes compared to Th22 cells (p<2.2e-16, linear mixed model, Fig. 4g) despite similar mRNA expression of *JUN* (p=0.81). Treatment with anifrolumab significantly reduced the proportion of cells in the Tph cluster (log_2FC −0.33, p=0.03, Fig. 4h) and increased the proportion of cells in the Th22 cluster (log_2FC 0.7, p=0.016, paired t-test). Taken together, these data indicate that type I IFN promotes Tph accumulation and CXCL13 production in SLE patients.

To test whether IFNs act directly on T cells to promote CXCL13, we stimulated CD4+ T cells from healthy donors in the presence or absence of IFN-α under varied AHR activation conditions (Fig. 4i). IFN-α increased T cell CXCL13 production in all cases and significantly decreased IL-22 production in cells treated with AHR agonist. The combination

Author Manuscript Author Manuscript Author Manuscript Author Manuscript

of IFN-α+AHR inhibition or deletion further amplified CXCL13 production, particularly in the presence of TGF-β (Fig. 4j).

To examine whether type I IFN induces a Tph epigenetic profile, we compared published ATAC-Seq data from $CD4^+$ T cells treated with IFN-β[29] with ATAC-Seq profiles of RA SF Tph cells and of $CD4^+$ T cells stimulated in the presence of an AHR inhibitor. This analysis revealed a significant overlap in chromatin accessibility among IFN-treated T cells with SF Tph cells (hypergeometric p=1.111e-06), AHR inhibitor-treated $CD4^+$ T cells (hypergeometric p=2.891e-08), and between all three groups (hypergeometric p=6.041e-14) (Fig. 4k) These overlaps were de-enriched in DAR upregulated in the T cells not treated with IFN-β. IFN-β treatment increased accessibility at the *CXCL13* locus (Fig. 4l). Moreover, IFN-β downregulated ATAC-Seq peaks in genes associated with AHR signaling (Extended Data Fig. 10b). These results suggested that type I IFN can function as a physiological AHR inhibitor. Supporting this idea, pretreatment of AHR reporter cells with IFN-β inhibited TCDD-induced luciferase activation (Fig. 4m). In addition, pre-treatment of human CD4 T cells with IFN-α inhibited TCDD-induced upregulation of *CYP1A1* (Extended Data Fig. 10c).

To identify potential mechanisms linking IFN signaling to Tph or Th22 cell differentiation, we performed an arrayed CRISPR screen targeting a set of IFN regulatory module genes in CD4+ T cells[29] (Fig. 5a). As expected, CRISPR deletion of IFN alpha/beta receptor 2 (*IFNAR2*) blocked IFN-induced CXCL13 upregulation. In addition, CRISPR deletion of *STAT5A*, *STAT1,* and *JAK1* increased CXCL13 and decreased IL-22 production, much like AHR deletion. While these genes have been implicated in IFN signaling[29], all 3 are also mediators of signaling by IL-2[30], a factor that suppresses CXCL13 production[13,14]. Consistent with this observation, Tph cells from SLE patients showed a low IL-2 response gene signature compared to Th22 cells (p=0.0175, LMM, Fig. 5b). *In vitro*, addition of IL-2 to memory $CD4^+$ T cells stimulated with anti-CD3 significantly decreased CXCL13 production and increased IL-22 production (Fig. 5c). This effect required STAT5, as CRISPR depletion of *STAT5A* and *STAT5B* blocked the effect of IL-2 on CXCL13 and IL-22 production (Fig. 5d). Addition of type I IFN to IL-2-treated $CD4^+$ T cells restored CXCL13 production, indicating that IFN can inhibit the ability of an IL-2-STAT5 axis to suppress CXCL13 production (Fig. 5e. IFN-β also reduced production of IL-2 from *in vitro* stimulated $CD4^+$ T cells (Fig. 5f, consistent with prior studies[31].

Finally, we investigated whether IFN influences JUN expression or function. Treatment of $CD4^+$ T cells with IFN-α significantly reduced expression of both phospho-JUN and total JUN (Fig. 5g). CUT&RUN analyses of JUN performed in $CD4^+$ T cells cultured with and without IFN-α demonstrated that IFN-α significantly reduced JUN binding across the genome, including at the *IL22* locus and at genes associated with Th17 and AHR signaling (Diffbind, FDR<0.1) (Fig. 5h,i, Supplementary Table 11). Lentiviral overexpression of JUN blunted the ability of IFN-α to augment CXCL13 and repress IL-22 production (Fig. 5j). Together, these results highlight a potent effect of IFN in controlling accumulation of a $CXCL13^+$ T cell population in SLE patients, with effects at multiple levels to oppose AHR-, IL-2-, and JUN-mediated repression of a $CXCL13^+$ phenotype (Fig. 5k.

Author Manuscript Author Manuscript Author Manuscript Author Manuscript

Discussion

Here we describe a dysregulated balance of reciprocally related Tph/Tfh and Th22 phenotypes in patients with SLE. This axis is strongly controlled by AHR, which acts in concert with JUN to block differentiation of CXCL13$^+$ Tph cells and promote IL-22$^+$ Th22 cells. Insufficient AHR activation has been suggested in SLE and other autoimmune contexts[18,32,33]; our results implicate IFN as an endogenous inhibitor of AHR actions at multiple levels. Type I IFN also inhibits JUN expression and disrupts JUN binding to multiple sites across the genome. This IFN-mediated inhibition of AP-1 may allow Tph cells to acquire B cell-helper functions despite low expression of BCL6, a transcription factor that inhibits AP-1 activity to allow full differentiation and function of Tfh cells[34,35]. The ability of IFNAR blockade to reduce levels of Tph cells and CXCL13 in lupus patients strongly implicates IFN in this pathway *in vivo*. Notably, several factors that regulate CXCL13$^+$ Tph cells appear to be shared with exhausted CD4+ T cells[36] and antigen-reactive CXCL13$^+$ CD8$^+$ T cells in the tumor microenvironment[37,38]. Like CD4$^+$ Tph cells in SLE, CXCL13$^+$ CD8$^+$ T cells in tumors appear chronically TCR-activated, deficient in JUN[39], exposed to TGF-β and/or type I IFN, and deprived of IL-2, a factor that can promote intrinsic AHR signaling[40].

Our results suggest that augmenting AHR activation therapeutically may prevent CXCL13$^+$ Tph/Tfh differentiation and the subsequent recruitment of B cells and formation of lymphoid aggregates in inflamed tissues[41]. Boosting Th22 cell generation may also have benefits in mucosal barrier integrity in SLE[42,43], though potential inflammatory consequences are possible[44]. Collectively, these data support the therapeutic potential of AHR agonism for autoimmune diseases, either systemically or directed towards T cells.

Methods

Human subjects research

Human subjects research was performed according to the Institutional Review Board at Mass General Brigham (IRB protocol 2014P002558, 2018P001961, 2021P002267) via approved protocols with informed consent as required. Synovial fluid samples were collected from patients with RA as discarded fluid from clinically indicated arthrocentesis. Seropositive (RF+ and/or anti-CCP+) RA patients fulfilled 2010 ACR/EULAR classification criteria. SLE patients fulfilled the 2019 ACR/EULAR criteria[45]. Blood samples were obtained from individuals with SLE, RA, as well as individuals without inflammatory diseases. Mononuclear cells from synovial fluid and peripheral blood were isolated by density centrifugation using Ficoll-Paque Plus (GE healthcare) and cryopreserved in FBS + 10% DMSO by slow freeze, followed by storage in liquid nitrogen for batched analyses. For experimental analyses, cryopreserved samples were thawed into warm RPMI medium + 10% FBS.

Mass cytometry staining

Samples were processed in 3 batches, including balanced numbers of SLE and control samples per batch. Cryopreserved cells were thawed and trypan blue negative viable cells

Author Manuscript Author Manuscript Author Manuscript Author Manuscript

were counted by hemocytometry. Approximately 1 million live cells per sample were used for mass cytometry staining. All antibodies were obtained from the Longwood Medical Area CyTOF Core. Buffers were from Fluidigm. Cells were stained with rhodium (Fluidigm) for viability then washed. Cells were washed and stained with primary antibody cocktails at a dilution of 1:100 using custom metal-conjugated antibodies obtained from the Longwood Medical Area CyTOF Antibody Resource Core (Boston, MA). Cells were then washed, fixed and permeabilized using the Ebioscience Transcription Factor Fix/Perm Buffer for 45 min, washed in PBS/1% BSA/0.3% saponin, then stained for intracellular markers. Cells were re-fixed in formalin (Sigma), washed with Milli-Q water, and analyzed on a CyTOF2 (Fluidigm). Mass cytometry data were normalized using EQ Four Element Calibration Beads (Fluidigm).

Mass cytometry data analysis

Normalized FCS files were uploaded in FlowJo v.10.4.2. Live singlet cells were determined by manual gating and normalization beads were excluded. FCS files including all manually gated T CD4 memory cells (CD3+CD8-CD4+CD45RO+) were uploaded and read in R (v.4.0.3) using the flowCore package. Marker expressions were arcsinh transformed using a co-factor of 5. The transformed matrix of expression was transposed and implemented into a Seurat object with the corresponding metadata. To check data quality, we verified the distribution of the markers across the three batches and confirmed minimal batch effect. From the 30 initial markers, we selected 18 of them that were non-redundant in each sample and variable across samples, as determined by the PCA-based non-redundancy score[46]. To ensure equal representation of samples and conditions (SLE versus controls) for further unsupervised analysis, we downsampled randomly to 2000 cells/sample. The data was then processed and analyzed using the Seurat pipeline (Seurat package v.4.1.1). We used the functions ScaleData and RunPCA with the default settings. The nearest-neighbor graph was built using the function FindNeighbors on the 10 first principal components followed by a Louvain-based clustering analysis (function FindClusters) with a resolution of 0.5. To visualize the data, we used UMAP as a dimensionality reduction tool (runUMAP) based on the 10 first principal components.

To compare cell abundances within T CD4 memory between SLE and control samples we first applied CNA[15] using its R implementation for Seurat (rcna package v.0.0.99). CNA defines the abundance of cells from each sample within defined neighborhoods (small groups of cells based on the nearest-neighbor graph) and applies PCA to the neighborhood abundance matrix for dimensionality reduction. Association testing is then performed with a specified clinical feature using a linear model. CNA was used here to capture small groups of cells that co-vary with SLE disease (control = 1, SLE = 2), while controlling for age, sex and batch Figure 1C). In addition to CNA, we used Mixed-effects Association testing for Single Cells (MASC)[47], an approach previously validated for mass cytometry analysis testing cluster attribution and association with a specific clinical variable. Here we used MASC to test for the contribution of SLE (versus control) to cluster membership for each single cell. We defined SLE versus control as the contrast variable, age and sex as fixed factors and patient and batch as random factors (Figure 1D, Supplementary Figure A right panel). MASC determines an odds ratio (and 95% confidence intervals) for SLE

Author Manuscript Author Manuscript Author Manuscript Author Manuscript

disease for each clusters. P values were then adjusted for multiple testing using Bonferroni's correction. Manual biaxial gating was performed using FlowJo (v.10.4.2) for quality control and independent examination of the expression of markers and frequencies of populations.

In vitro culture of human T cells

Total or memory CD4+ T cells were isolated from PBMC by negative selection using magnetic beads (Miltenyi Biotec). Alternatively, CD4+ T cells were isolated by magnetic positive selection using Dynabeads (Invitrogen #11331D). CD45RO+ memory CD4 T cells were further isolated from bulk CD4+ T cells by negative selection, depleting CD45RA+ naïve CD4 T cells using CD45RA mouse IgG antibodies (Invitrogen #14–0458-82) and Pan IgG Dynabeads (Invitrogen #11531D). Cells were cultured in complete RPMI consisting of RPMI-1640 medium (Gibco #21875034), 10% FBS, 1% penicillin/streptomycin, 10mM HEPES, 1% L-glutamine. In some cases, the 1% L-glutamine was replaced with 1mM sodium pyruvate. For *in vitro* culturing with AHR modulation, T cells were cultured in complete RPMI medium with Dyna anti-CD3/CD28 T activator beads (Invitrogen #11131D) at 1:5 bead:cell ratio with 2ng/mL human TGF-b1 (Peprotech #100–21C R&D 7754-BH-025), and either 10μM of CH-223191 (Sigma C8124) or 3–5nM of TCDD as indicated (AccuStandard, #1746–01-6). For experiments with IFN-α or IFN-β, 1000U/mL of IFN-α (R&D PHC4814) or IFN-β (Peprotech #300–02BC) were added. For experiments with IL-2, unless indicated, 10ng/mL of IL-2 (Peprotech #200–02) was added to complete RPMI medium and cells were either stimulated with CD3/CD28 T activator beads or plate-bound anti-CD3 antibodies (Thermo #16–0036-81, clone SK7).

CRISPR-Cas9 Delivery

Electroporation of human CD4+ T cells with CRISPR-Cas9-gRNA ribonucleoprotein (crRNP) complexes was performed as previously described[48] with minor modifications. Briefly, guide RNAs were designed using CRISPick online design tool by Broad Institute or ITDNA[49] and purchased from Integrated DNA technologies (IDT, Alt-R CRISPR Cas9 crRNA). crRNAs were duplexed with tracrRNA (IDT #1072534) for 2 minutes at 95°C or 40minutes at 37°C in 5% CO_2 incubator and complexed with Cas9 protein (Macrolab, Berkeley, 40μM stock) at 1:2 or 1:1 molar ratio for up to 60 minutes at 37°C. After 48–72 hours of stimulation with Dyna CD3/CD28 T activator beads, cells were collected, stripped from beads, pelleted, and resuspended in Lonza electroporation buffer P3 (Lonza #V4XP-3032) at 0.2–2M 10^6 cells / 20μL. Cells were electroporated in 16-well cuvettes using pulse code EH115 (Lonza #AAF-1002X). 100μL of pre-warmed complete RPMI culture media was added and cuvettes were incubated at 37°C and 5% CO_2 for 15 minutes. Cells were then transferred to 48 or 96-well plates containing complete RPMI media and CD3/CD28 T activator beads.

CRISPR Arrayed Screen

Custom 96-well CRISPR array library plates were purchased from Horizon Discovery Ltd. Each well consisted of 4 individual gRNA guides targeting the same gene. Ribonucleoprotein (crRNP) complexes were made from gRNA from each well as previously described[48], and aliquoted and stored at −80°C in lo-bind plates (Eppendorf). Electroporation of pre-stimulated T cells was done as described above. Non-targeting guides

Author Manuscript Author Manuscript Author Manuscript Author Manuscript

CD8a, *CD19* and *OR1A1* sgRNAs were included as controls in the CRISPR-Cas9 screen. Roughly 60 million memory CD4+ T cells were stimulated with anti-CD3/CD28 Dyna activator beads for 72 hours prior to electroporation. On day of electroporation, stimulator beads were removed, and cells were resuspended in electroporation buffer P3 (Lonza) at 0.5–0.7 million cells / 20μL, pipette mixed with crRNP complexes in lo-bind plate, transferred into 96-well Nucleofector™ plate (Lonza #V4SP-3096), and electroporated using 96-well Shuttle™ (Lonza). Immediately after electroporation, 80μL of pre-warmed complete RPMI culture media was added to each well of the Nucleofector™ plate and rested in incubator at 37°C and 5% CO_2 for 15 minutes. Cells were then transferred to 96-well plates containing complete RPMI media and anti-CD3/CD28 T activator beads and incubated at 37°C and 5% CO_2 for 4 days, supplementing 100μL of fresh complete RPMI on day 3. After 4 days, cells were resuspended with gentle pipetting, and 20μL was removed for cell count using CountBright™ beads (Invitrogen #C36950). Roughly 0.3 million cells were removed from each well to make protein lysates for CRISPR knockout verification as previously described[48]. Remaining cells were split evenly between two new 96-well plates for culture conditions of anti-CD3/CD28 bead stimulation with or without TGF-β1 (2ng/mL). Cells were cultured for 8 days after splitting into new conditions, and 100μL of supernatants collected on days 4, 6 and 8 of culture. 100μL of fresh complete RPMI with or without TGF-β1 was re-added to respective culture plate after each supernatant collection. For AP-1 family transcription factor screen, cells were cultured in 4 different conditions of anti-CD3/CD28 bead stimulation with either DMSO, DMSO with TGF-β1 (2ng/mL), TGF-β1 with AHR inhibitor (CH-223191, 10μM), or TGF-β1 with AHR agonist (TCDD, 3nM). For IFN-α screen, cells were cultured with anti-CD3/CD28 bead stimulation with either PBS or IFN-α (1000U/mL).

Cleavage Under Targets & Release Using Nuclease (CUT&RUN)

CUT&RUN[50] was performed using the CUTANA ChIC / CUT&RUN Kit (EpiCypher #14–1048) and following manufacture protocol with minor modifications. Briefly, human CD4 memory T cells were isolated and stimulated for 72 hours with TGF-β1 and either AHR agonist or AHR antagonist, or in a separate experiment with either PBS or IFN-α. T cells were then collected and washed in wash buffer provided by kit. Cells were then incubated with activated ConA beads for 10 minutes at room temperature. Bead bound cells were resuspended in kit-provided antibody buffer supplemented with 0.1% bovine serum albumin, 100nM trichostatin A, 0.1 U citrate synthase, and 1mM oxaloacetic acid. Cells in antibody buffer were incubated with antibodies targeting either AHR (1:25, CST #83200), JUN (1:25, CST #9165), or IgG control (1:100, Epicypher #13–0042) overnight on nutator at 4°C. The following day, cells were washed with cell permeabilization buffer twice and incubated with pAG-Mnase for 1 hour on nutator at 4°C. After incubation, cells were washed and while on ice, 100mM calcium chloride was added to each sample and incubated for 1 hour on nutator at 4°C. Finally, cells were incubated at 37°C for 30 minutes for DNA release, and DNA was cleaned and concentrated using the kit-provided DNA purification buffers and columns. DNA quantity was measured using Qubit dsDNA HS assay kit (Invitrogen #Q32851) and Qubit 2.0 fluorometer (Invitrogen). CUT&RUN library prep was performed using KAPA HyperPrep Kit (Roche), and paired-end DNA sequencing was performed on a HiSeq 2500 platform (Illumina) at Admera Health Inc.

Author Manuscript Author Manuscript Author Manuscript Author Manuscript

CUT&RUN Data analysis

Raw CUT&RUN Sequenced reads (FASTQ files) were processed using script adapted and modified from the following repository: https://github.com/wherrylab/jogiles_ATAC. Briefly, samples were aligned to human genome hg38 (GRCh38) using Bowtie 2 (v.2.2.6). Samtools was used to remove unmapped, unpaired and mitochondrial reads. ENCODE blacklist regions were also removed (https://sites.google.com/site/anshulkundaje/projects/blacklists). PCR duplicates were removed using Picard. Peak calling was performed using SEACR (v.1.3) in relaxed setting normalized to IgG control. The number of reads in each peak was determined using BedTools coverage. Peak annotation was performed using ChIPseeker[51] package (v.1.30.3) in R (v.4.1.1). Differentially bound peaks were identified using Diffbind package (v.3.4.11) in R, following DESeq2 (v.1.34.0) normalization using an FDR cut-off <M0.05 unless otherwise indicated. Tracks were visualized using Integrative Genomics Viewer (IGV, v.2.13.0, Broad Institute). Motif enrichment analysis and gene-to-peak association was performed using HOMER (v.4.10) with default settings. Significance in overlapped genes or bound regions was calculated with hypergeometric tests. P values and q values <0.05 were considered to indicate a significant difference. Tracks shown in figures were generated on IGV using bigwig files.

Time-course RNA-Seq experiment and module analysis

RNA from human memory CD4 T cells was isolated from cells (200,000 cells) stimulated with anti-CD3/CD28 Dyna beads and cultured in TGF-b1 with either AHR antagonist or agonist for 12, 24, 48 and 72 hours. RNA was isolated with Rneasy Plus Micro Kit (Qiagen #74034) following manufacture protocol. RNA libraries were prepared using the QuantSeq FWD Kit for Illumina Sequencing (Lexogen) for 3'RNA-Seq. Sequencing was performed on Illumina NextSeq platform. Three biological replicates of each sample were sequenced. Sequence quality was assessed with FastQC (v.0.11.5), FASTQ files were trimmed using BBduk from BBMap (v.38.90) according to Lexogen QuantSeq manufacturer's parameters, and mappged to hg38 using STAR (v.2.6.0). HTSeq was used to count uniquely mapped reads and significantly differentially expressed genes at each time point were determined using DESeq2. Time-course analyses were performed using maSigPro[52] using default settings. Volcano plots and PCA plots were generated using R (v.4.1.1).

Lentiviral Transduction of Human T cells for JUN overexpression

cDNA encoding c-JUN (*JUN*) was reverse transcribed from total mRNA isolated from activated primary CD4 T cells and cloned into lentiviral expression vector (System Bioscience #CD511b-1) to create JUN overexpressing vector. *JUN* open reading frame (ORF) was subcloned into the EcoRI site of lentiviral vector using Gibson Assembly (NEB). JUN overexpressing vector was transformed into NEB Stable (NEB #C3040H) chemically competent cells and purified ZymoPURE plasmid Midiprep kit (Zymo Research #D4201-A). Pantropic. VSV-G pseudotyped lentivirus was produced via transfection of 293T cells with JUN overexpression vector and the viral packaging plasmids pCMVdr8.91 and pCMV-VSV-G using FuGENE (Promega #E2311). Primary CD4 memory T cells were isolated as described above, on the same day of 293T cell transfection. After 24 hours in culture, memory T cells were stimulated with CD3/CD28 T-activator Dynabeads (Life Technologies

Author Manuscript Author Manuscript Author Manuscript Author Manuscript

#11131D) at a 1:2 bead:cell ratio. At 48 hours, viral supernatant was harvested, filtered, concentrated, and added to primary T cell culture for 24 hours. At day 5 post T cell stimulation, Dynabeads were removed and T cells were re-cultured in AHR modulating conditions with or without TGF-β for 8 days while supernatants were collected on days 4, and 8 for ELISA assays.

For CUT&RUN and RNA-Seq of JUN overexpressing cells, cells were sorted at day 5 post T cell stimulation based on GFP positivity. Sorted cells were cultured for 72 hours before being processed for CUT&RUN and RNA-Seq.

Flow cytometry staining

Cryopreserved cells were thawed, washed and counted. Cells ranging from 0.1–2 million cells were stained in PBS with Aqua fixable live/dead dye (Invitrogen) for 20 minutes at 4 °C.

For surface staining, cells were stained in PBS with 1% BSA with the following antibodies for 20–30 minutes at 4°C with indicated dilution: anti-CD3 BV711 (OKT3) 1:100, anti-CD3 A700 (OKT3) 1:100, anti-CD4 Pe-Cy7(RPA-T4) 1:100, anti-CD8 BV510 (RPA-T8) 1:100, anti-CD56 BV510 (HCD56) 1:100, anti-CD25 FITC (M-A251) 1:20, anti-CD25 PerpCy5.5 (M-A251) 1:20, anti-CD127 Alexa Fluor 700 (A019D5) 1:20, anti-CD127 APC (A019D5) 1:20, anti-CXCR5 BV421 (J252D4) 1:20, anti-PD-1 BV711 (EH12.2H2) 1:100, anti-ICOS FITC (C398.4A) 1:20, anti-IL-17A PB (BL168) 1:40, anti-IFN-γ (B27) 1:100, anti-TNF FITC (Mab11) 1:40, anti-CD14 APC (M5E2) 1:50, anti-CD3 Alexa700 (HIT3a) 1:100, anti-CD19 PE (HIB19) 1:100, anti-CD27 BV421 (O323) 1:50, and anti-IgD FITC (IA6–2) 1:50, anti-CD4 FITC (RPA-T4) 1:100, anti-CD19 APC-Cy7 (HIB19) 1:100, anti-CD27 PE-Cy7 (M-T271) 1:50, anti-CD38 BV785 (HIT2) 1:100 (all from BioLegend), anti-CD45RA APC-efluor788 (HI100) 1:100, LIVE/DEAD Fixable Aqua 1:100, anti-AHR (FF3399) 1:20, anti-IL-22 PeCy7 (22URTI) 1:20, anti-IL-4 APC (8D4–8) 1:20 (all from Invitrogen), anti-CD4 BUV395 (RPA-T4) 1:100 and anti-CD8 BUV395 (RPA-T8) 1:100 (BD Biosciences). Cells were washed in cold PBS 1% BSA. For intracellular or intranuclear staining, the eBioscience™ Foxp3 / Transcription Factor Staining Buffer Set (Thermofisher) was used. For detection of intracellular cytokines, depending on the experiment, cells were stimulated for 4 days with anti-CD3/CD28 Dyna beads (1:5 bead: cell ratio) or 10 days with Th1, Th2, Th17 polarization cocktails and then re-stimulated with 1x PMA/ionomycin (Invitrogen) for 6 hours. Brefeldin A (Invitrogen) was added 2 hours later and incubated with the cells for 4 hours. Cells were stained for viability and indicated surface markers as above. Following surface staining, cells were washed and incubated with 1xFixation/Permeabilization Buffer at room temperature for 40 minutes at 4°C. Cells were then washed in 1x eBioscience Permeabilization Buffer. For intracellular cytoplasmic staining, cells were incubated with indicated intracellular antibodies for 30min at 4°C. For intranuclear staining, cells were incubated with indicated intracellular antibodies for 1 hour at room temperature. Cells were then washed twice in 1x eBioscience Permeabilization Buffer and washed once more with PBS 1% BSA. Data acquired on a BD Fortessa analyzer using FACSDiva software and were analyzed using FlowJo (v.10.4.2).

Author Manuscript Author Manuscript Author Manuscript Author Manuscript

Flow cytometric cell sorting

We used 2 flow cytometry panels of 9 and 11 colors to identify memory CD4 T cell populations. Panel #1 included anti-CD3 BV510 1:100, anti-CD4 PE-Cy7 1:100, anti-CD45RA BV605 1:100, anti-CD25 FITC 1:20, anti-CD127 BV711 1:20, anti-PD-1 APC-Cy7 1:100, anti-CXCR5 BV421 1:20, anti-CD96 APC 1:20, anti-TIGIT PE 1:20. Panel #2 included anti-CD8 BV510 1:100, anti-CD19 BV510 1:100, anti-CD56 BV510 1:100, anti-CD25 FITC 1:20, anti-CD127 Alexa Fluor 700 1:20, anti-CD96 APC 1:20, anti-CXCR5 BV421 1:20, anti-TIGIT PE 1:20, anti-CCR6 BV605 1:20, anti-PD-1 BV711 1:100, propidium iodide (all from BioLegend), and anti-CD45RA APC-efluor780 1:100, anti-CXCR3 PE-Cy7 (Invitrogen) 1:20. Memory B cells were identified with this panel: propidium iodide, anti-CD14 APC 1:50, anti-CD3 Alexa700 1:100, anti-CD19 PE 1:100, anti-CD27 BV421 1:50 and anti-IgD FITC 1:100. Cells were incubated at 4°C with antibodies in PBS /1% BSA for 15–30 minutes. Cells were washed once in PBS/1% BSA, centrifuged and passed through a 70μM filter, and propidium iodide was added immediately prior to sorting. Cells were sorted on a 4-laser BD FACSAria Fusion cell sorter. Intact cells were gated according to forward scatter and side scatter area (FSC-A and SSC-A). Doublets were excluded by serial FSC-H/FSC-W and SSC-H/SSC-W gates (H, height; W, width). Non-viable cells were excluded based on propidium iodide uptake. Cells were sorted through a 70μM nozzle at 70 psi. Cell purity was routinely >98%. For functional analyses, 0.2–1 million cells were sorted from each population into cold RPMI/10% FBS. For RNA-Seq, up to 2000 cells were collected from each cell subset directly into buffer TCL (Qiagen) with 1% β-mercaptoethanol (Sigma). Flow cytometric quantification of cell populations was performed using FlowJo (v.10.0.7).

T:B co-culture assay

Tfh cells were flow sorted with panel #2 and activated with anti-CD3/CD28 Dynabeads in the presence of either DMSO, TCDD, or CH-223191 for 48 hours. Tfh cells were then collected and stained with LIVE/DEAD, and live Tfh cells were flow sorted again. In parallel, B cells were isolated from PBMCs from the same donor, and $CD27^{+}$ IgD^{-} memory B cells were flow sorted. Tfh and memory B cells were co-cultured in the presence of SEB (1ug/ml) for 5 days. Cells were then analyzed by flow cytometry to quantify $CD38^{hi}$ $CD27^{+}$ plasmablasts among B cells.

Th1/Th2/Th17 polarization

Naïve and memory $CD4^{+}$ T cells were stimulated with anti-CD3/CD28 Dynabeads for 4 days in Th1-polarizing conditions (IL-12 (10 ng/ml), IL-2 (20ng/ml) and anti-IL-4 Abs (1 μg/ml MAB204)) (R&D Systems), Th2-polarizing conditions (IL-4 (20 ng/ml), anti-IFNγ (1μg/ml MAB285) (R&D Systems), or Th17-polarizing conditions (IL-6 (50ng/ml), TGF-β (2ng/mL), IL-23 (40ng/mL), IL-1β (10ng/mL), anti-IFNγ (1μg/ml), anti-IL-4 Abs (1 μg/ml) (R&D Systems) in the presence of DMSO, TCDD (5nM) or CH-223191 (10μM). Cells were split every 2–3 days and replenished with media containing the Th1- or Th2-polarization cocktails together with AHR modulators for 6 additional days. Intracellular staining was performed as indicated.

Author Manuscript Author Manuscript Author Manuscript Author Manuscript

ELISA quantification

Cytokine levels from supernatant of T-cell culture or from patient serum were quantified by ELISA using Human DuoSet ELISA kits for CXCL13, IL-22, IFN-γ.

AHR Luciferase Assay

HEPG2 cells were obtained from Dr. Gary Perdew, Penn State University. Cells were first cultured in DMEM, 15% FBS, 1% penicillin/streptomycin at 37°C until reaching 70% confluence. Cells were then washed, counted, and cultured at a density of 70,000 cells in 96-well plate wells overnight. Cells were then incubated with 10% serum from healthy or SLE patients in RPMI 1640 overnight. The following day, cells were treated with trypsin (Gibco), rinsed, and washed at 800 rpm for 8 minutes. Cells were resuspended in DMEM and lysed with Dual-Glo Luciferase Assay System (Promega#, E2920). The luciferase activity was read with GloMax® Explorer Multimode Microplate Reader, Promega)

Western Blotting

Rabbit anti-JUN, anti-phospho-JUN (Ser73), anti-AHR, anti-β-actin, anti-tubullin, anti-cyclophilin B, anti-vincullin antibodies were purchased from Cell Signaling Technology. Cells were pelleted and lysed with Laemmli buffer 1X (Biorad #1610747) or RIPA buffer (Thermofisher #89901) for 1h at 4 degrees using a micro-tube shaker. Lysed cells were then centrifuged at >14000rpm for 10 min, and lysates stored at −80 degrees. Protein was measured using Pierce BCA assay (ThermoScientific #23225), according to manufacturer's instructions. Protein lysates were loaded in 10x Tris 10% or 12% Criterion™ TGX™ Precast Midi protein gels, transferred to Immun-Blot® PVDF membrane at 4C for 2 hours with 0.2 amps. Membranes were blocked either with 5% milk or 5% BSA for 1 hour, or EveryBlot Blocking Buffer (Bio-Rad) for 5 min and then incubated with primary antibody overnight (1:1000 for anti-AHR, 1:50,000 for anti-tubulin, anti-cyclophilin B, anti-vinculin or anti-β-actin). Membranes were then incubated with the horseradish peroxidase conjugate-labeled secondary antibody (goat anti-rabbit IgG H+L, Invitrogen) for 1–2 hours and then washed with TBS-T. Protein bands were detected by SuperSignal™ West Femto Maximum Sensitivity substrate (#34096; Thermo Fisher Scientific). Images were obtained and quantified via Chemi Doc and Image Lab Software (Bio-Rad).

Subcellular fractionation

Human embryonic kidney 293T (HEK293T) cells were separately transduced with GFP containing lentiviral construct either native or encoding HA-tagged AHR as described above. Transduced HEK293Ts were sorted based on GFP positivity. Cells were then cultured for 72 hours with either AHR agonist, AHR antagonist or vehicle control as above and then harvested for protein lysates. The Standard Cell Fractionation Kit (Abcam #ab109719) was used to collect the cytoplasmic and nuclear fractions, as per the manufacturer's instructions. The Pierce BCA Protein Assay (ThermoFisher, #23225) was used to quantify the protein concentration within the cytoplasmic and nuclear fractions, as per the manufacturer's instructions. Western blot was performed as described above.

Author Manuscript Author Manuscript Author Manuscript Author Manuscript

Co-immunoprecipitation

Human embryonic kidney 293T (HEK293T) cells were transduced with GFP containing lentiviral constructs encoding either HA-tagged AHR or 3xFLAG-tagged c-Jun as described above. Transduced HEK293Ts were sorted based on GFP positivity. Cells were cultured for 72 hours with either AHR agonist, AHR antagonist or vehicle control as above and then harvested for protein lysates using Pierce IP Lysis Buffer (ThermoFisher, #87787) containing Halt Protease Inhibitor Cocktail (ThermoFisher, #78429). The Pierce BCA Protein Assay (ThermoFisher, #23225) was used to quantify the protein concentration within the cytoplasmic and nuclear fractions, as per the manufacturer's instructions.

The 3xFLAG co-immunoprecipitation was completed with the ANTI-FLAG M2 Affinity Gel (Millipore Sigma, #A2220) and the HA co-immunoprecipitation was completed using Pierce Anti-HA magnetic beads (Fisher, #PI88836). Briefly, 250μg of protein was incubated with washed agarose slurry or magnetic beads overnight at 4°C as per manufacturer instructions. Incubated anti-Flag M2 agarose slurry was washed with 50mM Tris-HCl buffer supplemented with 150mM NaCL,pH 7.6 (Millipore Sigma, #524750) before eluting with 1x Laemmli Sample Buffer (Biorad, #161–0747) at 70°C for 10min. 1μL β-mercaptoethanol was added to eluted product before running on SDS-PAGE for Western blot. Separately, incubated anti-HA magnetic beads were washed with 0.05% Tween-20 in150mM NaCL, 50mM Tris-HCl buffer, pH 7.6 (Millipore Sigma, #524750) before eluting with acidic 0.1M glycine buffer solution, pH 2.0–2.8 and neutralized with UltraPure 1M Tris-HCl Buffer, pH 9.5. 4x Laemmli Sample Buffer (Biorad, #161–0747) and β-mercaptoethanol were added to elution product before running on SDS-PAGE for Western blot.

Single Cell RNA-Seq of in vitro stimulated cells

Sample preparation—Isolated memory CD4 T cells were cultured at 1×10^5 cell per well in a 96 well plate with 200ul of RPMI/10% FBS and stimulated with Dynabeads (ThermoFisher). As indicated, cells were cultured with DMSO alone, TGF-β (2ng/mL) and DMSO, CH-223191 (10μM), or TCDD (3nM). Cells were collected at day 6 cells, restimulated, and collected at day 13. Cell counts were normalized across conditions and stained with LIVE/DEAD™ Fixable Aqua Dead Cell Stain Kit (Invitrogen) and cell hashing antibodies specific for each condition and donor, pooled, and stained with TotalSeq-C Human Universal Cocktail (BioLegend). Viable cells were then flow sorted and subjected to encapsulation and library preparation at the BWH Center for Cellular Profiling via the 10X Genomics pipeline, with 24–30K cells loaded per run with 82–95% viability.

Single cell RNA-seq data processing and QC—Libraries were prepared according to the 10x Genomics User Guide and processed by Cell Ranger (v.6.1.1) workflow. FASTQ files containing gene expression and feature barcodes were aligned to the human genome hg38 (GRCh38). The filtered features, barcodes, and matrix files were imported into R and used to generate a Seurat object with Seurat package (v.4.3.0). Quality control was first performed filtering out cells with more than 10% mitochondrial reads and with <200 or >5,500 reads. Cells that passed the QC were log normalized and scaled. The Seurat object was then demultiplexed using the hashtag oligos. HTO reads were normalized and cells assigned a HTO ID using the HTODemux function from Seurat. Doublets were removed

Author Manuscript Author Manuscript Author Manuscript Author Manuscript

and the filtered cells were used to run PCA using the Seurat Package. To account for donor variation, the Seurat object for each timepoint was individually integrated utilizing Harmony (v.0.1.1), where each Seurat object was corrected by donor. The top 10 harmony embeddings were then used to generate a UMP and clustering was performed with a resolution of 0.7. Differentially expressed genes between the four culture conditions were identified using the FindMarkers function in the Seurat Package.

Symphony Mapping—The Rheumatoid Arthritis reference dataset was generated though the Accelerating Medicines Partnership (AMP)[20]. T cells were identified as described[20], and filtered for cells with mitochondrial read <20% and with reads >200 and <5000. Cells passing filtering were normalized, scaled, and run though Harmony (v.0.1.1) integration correcting for donor. The top 15 harmony embeddings were used to generate a UMAP and clustered with a resolution of 0.8. The harmonized object was then used to generate a reference object with the buildReferenceFromSeurat Function in the Symphony package (v.0.1.1)[53]. Data from day 13 *in vitro* single cell data was then query mapped to the AMP reference. The frequency at which cells mapped to a given cluster was extracted and compared between culture conditions by donor.

Single Cell RNA-Seq of T cells from patients with lupus

Sample collection—Blood samples were also obtained from patients with SLE (n=5) or with a diagnosis of refractory cutaneous lupus (n=2) before starting treatment with anifrolumab (first day of infusion) and 1–3 months after the starting date. Cryopreserved PBMC were thawed, resuspended in Fc Receptor block (BioLegend) and then stained with hashing antibodies specific for each donor and timepoint, CD3-APC (BioLegend), and propidium iodide. Viable CD3+ T cells were flow-sorted, pooled, and stained with TotalSeq-C Human Universal Cocktail (BioLegend). Cells were then subjected to encapsulation and library preparation at the BWH Center for Cellular Profiling via the Chromium X system from 10X Genomics, with 2×100k cells loaded with 89% viability.

Anifrolumab single cell data analysis—Quality control was first performed filtering out cells with more than 15% mitochondrial reads and with <1,000 or >4,000 reads. Samples were demultiplexed and clustered as above, and memory CD4 T cells were selected for further analysis. Cells passing filtering were normalized, scaled, and run though Harmony (v.0.1.1) integration correcting for donor and 10x sequencing batch. The top 20 harmony embeddings were then used to generate a UMAP and clustering was performed with a resolution of 1.2. The signature scores are calculated using addmodulescore function from Seurat package.

Low-input bulk RNA-Seq analysis

Low input bulk RNA-Seq libraries were prepared at Broad Technology Labs at the Broad Institute of Harvard and MIT using the Illumina SmartSeq2 platform. Libraries were Sequenced to generate 38 base paired-end reads. FASTQ files from sequencing were examined with FastQC for quality control and trimmed with trimmomatic. Reads were aligned to human genome hg38 (GRCh38) using hisat2 alignment program. Lowly expressed genes (log2 FPKM<10 in 10 samples) were filtered out for downstream analysis.

Author Manuscript Author Manuscript Author Manuscript Author Manuscript

Differentially expressed genes (DEGs) were identified using DESeq2 with an adjusted p-value threshold of < 0.05. Principal component analysis (PCA) was performed using the prcomp function in R. The top 20% most variable genes were selected for this analysis. Heatmap is generated using the pheatmap package (v.1.0.12) in R using FPKM values that have been scaled by each gene. The signature genes for Tregs, CD96hi cells, or Tph/Tfh cells are the common DEGs in individual comparisons with each of the other cell groups. The ssgsea score is calculated by gsva package (GSVA v.1.38.2) in R. The Th22 cell gene signature list and Tph cell gene signature list were derived from previous reports[54,55].

ATAC-Seq data analysis

Raw sequencing data were trimmed using cutadapt (v.1.18) with Python (v.2.7.15) to remove the adapter. Trimmed reads were aligned to the GRCh38 human reference genome with Bowtie2; Aligned reads were filtered to remove mitochondrial reads and PCR duplicates, then peaks were called using Genrich in ATAC-Seq mode on individual samples. The fragment size distribution is checked using deepTools (v.3.1.2). The intervals were set to the default length of 100bp, and the peak-calling significance threshold was set to -log(p) > 2. A union peak list for each data set was created by combining all peaks in all samples, merging overlapping peaks using bedtools (v.2.26.0), and retaining only peaks that were called in more than one sample. Normalized read counts for consensus peaks were computed for each sample using Diffbind, and differential accessibility between different groups was determined using a matched pairs t-test with the edgeR package (v.3.30). Peaks were annotated using ChIPseeker (v.1.26.2). Enrichment analysis of peaks and Gene Sets Enrichment Analysis was conducted using the clusterProfiler (v.3.16) package with a threshold of FDR < 0.05 to define enriched pathways. For ATAC-Seq GSEA, peaks were declared differentially accessible at the genome-wide level with a false discovery rate adjusted p-value < 0.05, and those exhibiting a log2 fold change of ± 2 or greater were defined as $PD1^{hi}$ signature in tonsil and SF. The $PD\text{-}1^{hi}$ signatures were used for GSEA analysis using the clusterProfiler(v3.16) package. Peak signal tracks were generated using the rtracklayer package (v.1.48) or IGV software.

SLE patient plasma CXCL13 comparison from TULIP-1 randomized clinical trial

Circulating plasma samples taken at baseline, Week 12, and Week 52 (end of trial) from 302 patients in the TULIP-1 trial[28] were assessed for protein biomarkers by targeted high-multiplex immunoassay panels on the Olink platform; Olink Target 96 Immuno-Oncology (v.3112). Data for CXCL13 protein is presented as relative Normalized Protein eXpression (NPX), which is on a Log2 scale. Statistical analysis and data visualization conducted using standard packages in R version 4.0.1.

A longitudinal mixed effect model was used to test whether 1-year trajectory of CXCL13 protein were statistically different between anifrolumab and placebo arms. Model was adjusted for the trial stratification factors; baseline oral corticosteroid dose (<10 mg/day, ≥10 mg/day), Systemic Lupus Erythematosus Disease Activity Index 2000 (SLEDAI 2K) score at screening (<10 points, ≥10 points), and IFN 4-gene status[56]. Multiple testing was accounted for using the Benjamini-Hochberg (FDR) procedure with < 0.05 threshold.

Author Manuscript
Author Manuscript
Author Manuscript
Author Manuscript

Statistics

Statistical analysis was performed as described in each section and figure legends using Graphpad Prism 8 software and R (v.4.0.3). Unless otherwise indicated, multi-group analyses were performed using non-parametric Friedman test with Dunn's multiple comparisons test, and two group comparisons were performed using either paired t-test, Wilcoxon test or paired ratio t-test as indicated in figure legends. All tests were performed as two-sided tests, with $p<0.05$ considered significant. Correction for multiple testing was used only where indicated, and control for false discovery rate was calculated by Benjamini-Hochberg method.

Extended Data

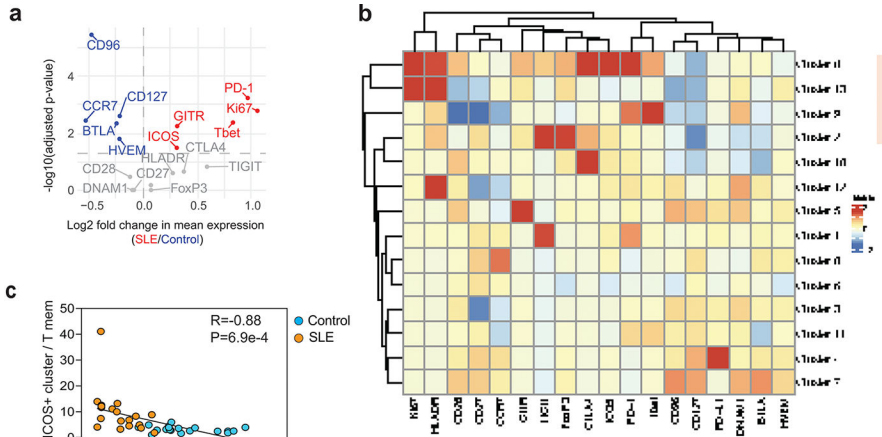

clusters	size	adj. model p value*	SLE OR	95% CI
7	5224	3.13e-09	0.3	0.2 - 0.4
2	7816	3.31e-05	2.1	1.60 - 2.6
8	4939	0.0002	2.8	1.90 - 4.2
0	11622	0.0026	0.5	0.4 - 0.7
11	2467	0.0971	0.7	0.5 - 0.9
6	5562	0.2543	0.8	0.6 - 0.9
5	5690	1.000	1.4	1.0 - 2.0
9	3803	1.000	3.0	1.2 - 8.0
3	7580	1.000	0.8	0.6 - 1.0
10	2496	1.000	0.9	0.7 - 1.1
12	1783	1.000	1.3	0.8 - 2.0
4	6919	1.000	0.9	0.7 - 1.1
13	405	1.000	0.6	0.2 - 2.0
1	9694	1.000	0.9	0.8 - 1.1

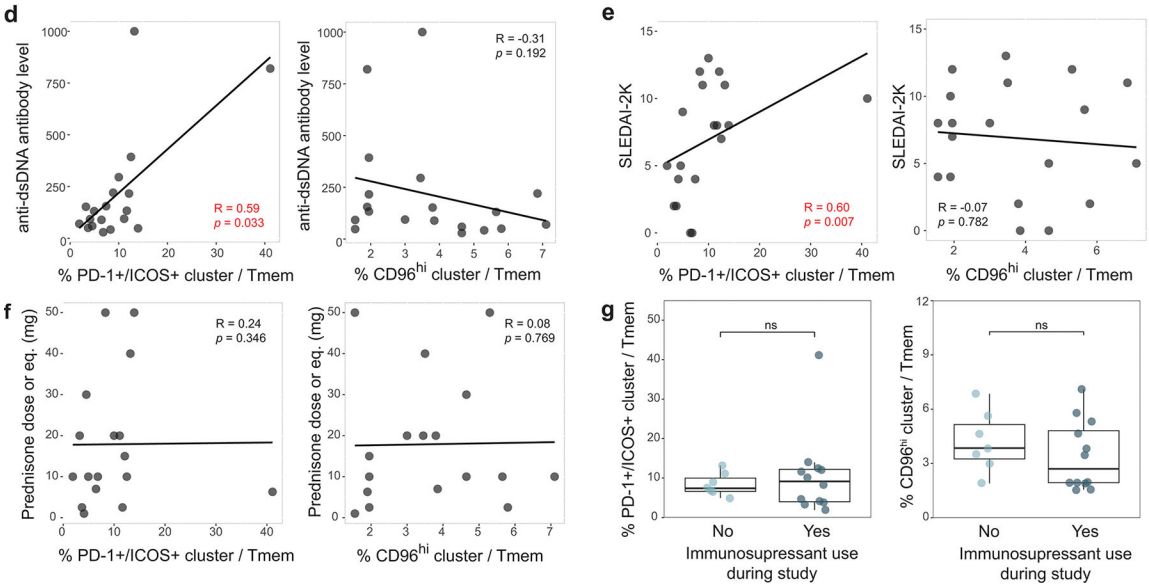

Extended Data Figure 1. Clinical associations of PD-1^{+}/ICOS^{+} and CD96^{hi} cell clusters.

Author Manuscript Author Manuscript Author Manuscript Author Manuscript

a, Differentially expressed proteins on memory $CD4^+$ T cells from SLE patients compared to controls. p-values from t-test with Bonferroni correction. **b**, Heatmap of marker expression on mass cytometry cell clusters (left) and MASC association statistics for each cluster comparing SLE vs controls (right). SLE OR = odds ratio of representation in SLE vs control. CI = confidence interval. Adj. p-value by FDR. **c**, Correlation plot of PD-1/ICOS+ cluster and $CD96^{hi}$ cluster abundances in SLE patients and controls. Spearman statistics shown. **d**, Association of indicated cluster proportions with serum anti-dsDNA antibody level in SLE patients (n=19). **e**, Association of indicated cluster proportions with SLE disease activity by SLEDAI-2K (n=19). **f**, Association of indicated cluster proportions with prednisone dose or equivalent at time of sample collection. **g**, Cluster proportions of $PD\text{-}1^+$/$ICOS^+$ (left) and $CD96^{hi}$ (right) clusters in SLE patients stratified by immunosuppressant drug use at time of sample collection (no, n=7; yes, n=12). Spearman correlation statistics shown in **d**-**f**. Boxes in **g** show median ± interquartile, with bars indicating min/max values within 1.5x interquartile range. Statistics by Mann-Whitney test.

Author Manuscript Author Manuscript Author Manuscript Author Manuscript

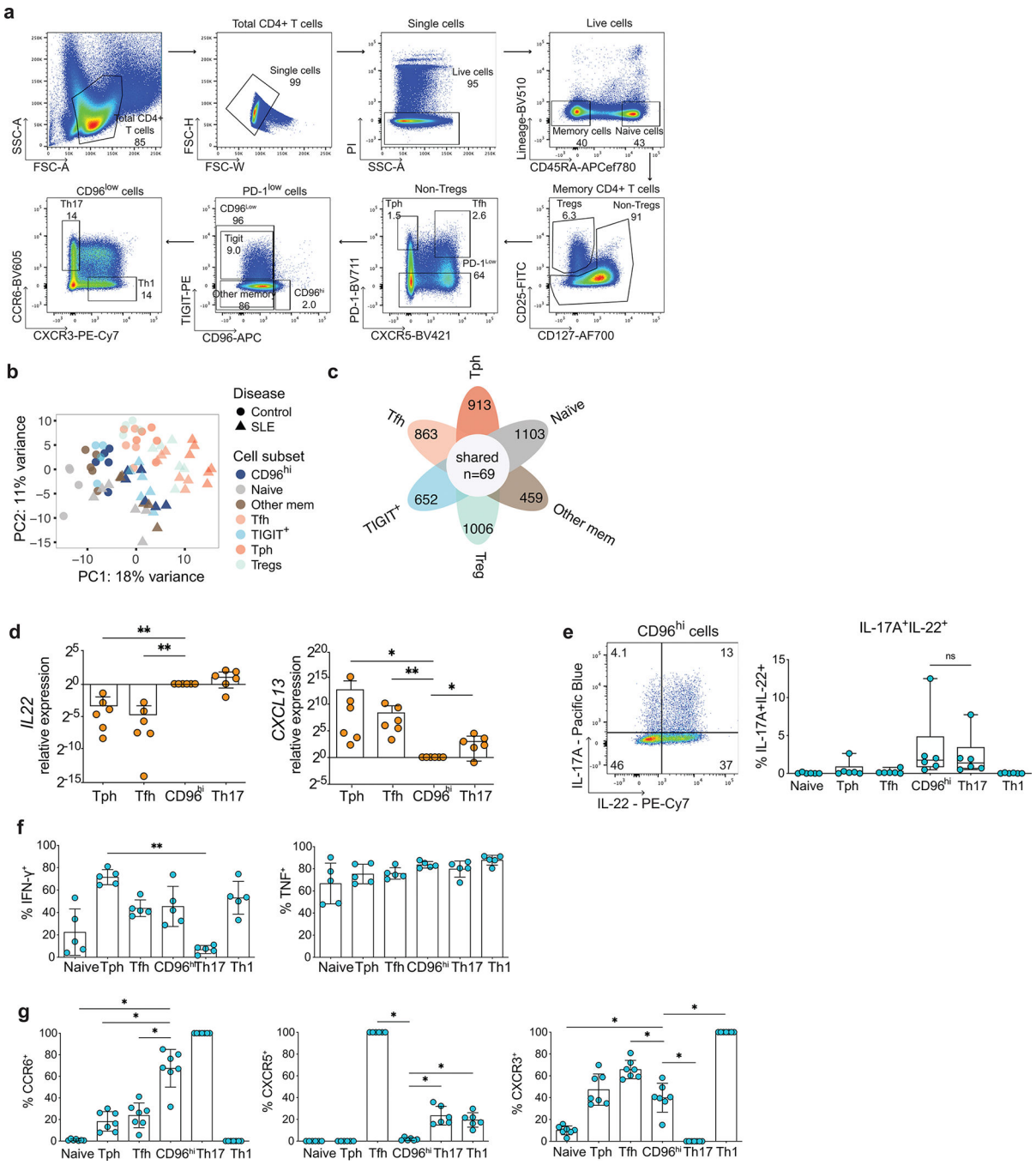

Extended Data Figure 2. CD96^{hi} cells are a Th22 cell population.

a, Example of flow cytometry sorting of CD4^{+} T cell subsets for bulk RNA-seq analysis. **b**, PCA plot of bulk RNA-seq profiles of CD4^{+} T cell subsets sorted from SLE (n=6) or healthy control (n=5) donors. Colors indicate cell subsets and shapes indicate clinical group. **c**, Multi-set Venn diagram of the number of differentially expressed genes between CD96^{hi} cells and indicated CD4^{+} T cell subsets. **d**, Expression of *IL22* and *CXCL13* by qPCR in T cell populations from SLE patients (n=6), plotted relative to expression in CD96^{hi} cells. *IL22* expression p-values from left to right: 0.0063, 0.0075. *CXCL13* expression

Author Manuscript Author Manuscript Author Manuscript Author Manuscript

p-values from left to right: 0.0128, 0.0012, 0.0283. **e**, Flow cytometry detection of IL-22 and IL-17A in PMA/ionomycin-stimulated $CD96^{hi}$ CD4 T cells (left) and quantification of $IL\text{-}22^{+}$ $IL\text{-}17A^{+}$ cells (right) in cell subsets from controls (n=6). Boxes indicate median bounded by 1^{st} and 3^{rd} quartile; bars indicate min/max. **f**,**g**, Flow cytometry quantification of cytokines from PMA/ionomycin stimulated $CD4^{+}$ T cell subsets sorted from healthy donors (**f**, n=5, p=0.0012 for Th17 versus Tph) and base chemokine receptor expression (**g**, n=6–7). p-values for **g** from left to right, all comparing to $CD96^{hi}$ subset, for CCR6: 0.0156, 0.0156, 0.0156, for CXCR5: 0.0313, 0.0313, 0.0313, for CXCR3: 0.0156, 0.0156, 0.0156. Data for **f** and **g** are shown as mean ± S.D. *P*-values (*p<0.05, **p<0.01, ***p<0.001, ****p<0.0001) were obtained by ratio paired t-test in **d, f, g** or by Wilcoxon test in **e**.

Author Manuscript Author Manuscript Author Manuscript Author Manuscript

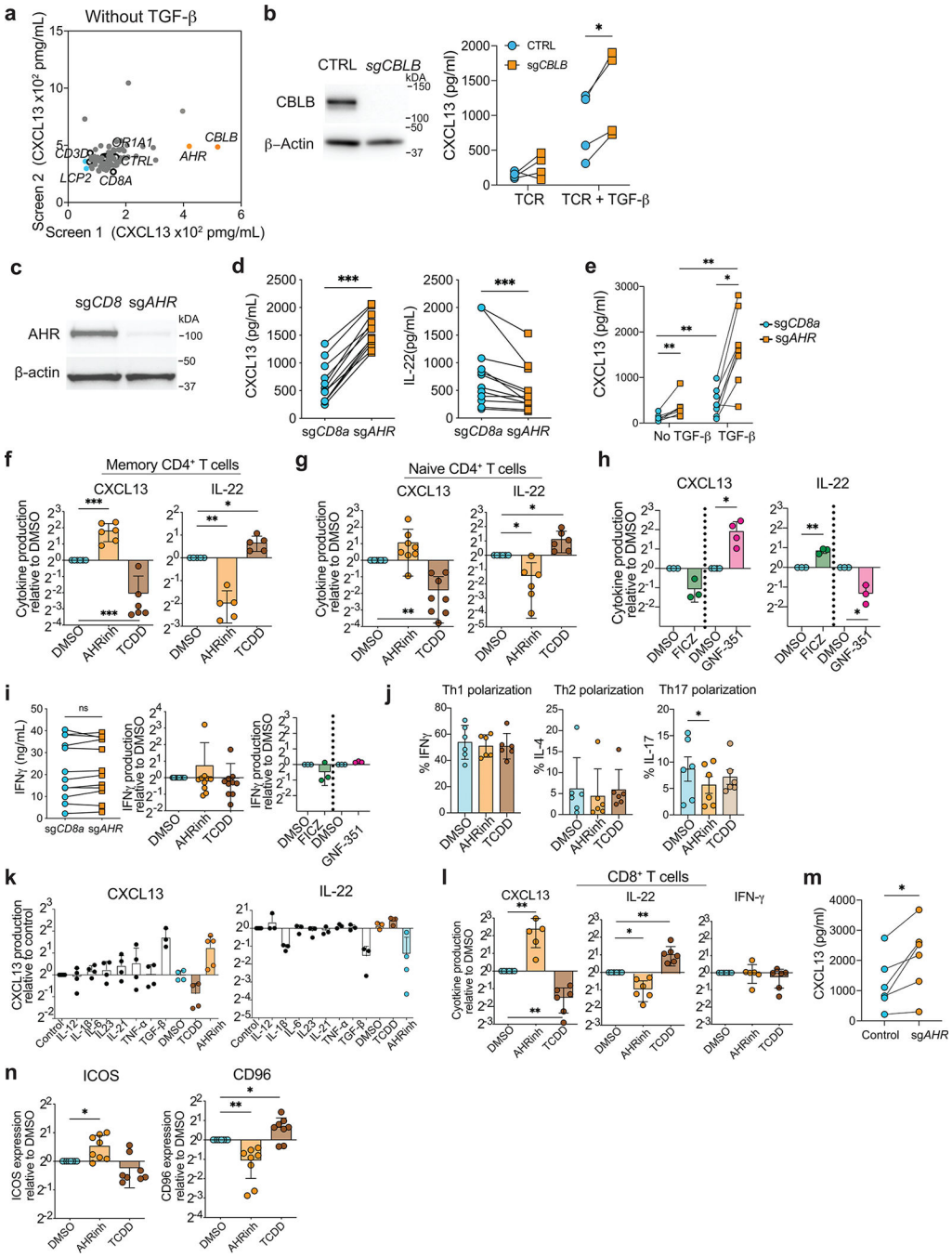

Extended Data Figure 3. AHR controls T cell production of CXCL13.

a, CXCL13 quantification by ELISA from cells in CRISPR screen without TGF-β. Results from 2 independent experiments using different donors. **b,** Western blot for CBLB in memory CD4$^+$ T cells treated with control or sgCBLB CRISPR guide (left) and ELISA quantification of CXCL13 from indicated cells (n=4, 2 biological donors each with 2 technical replicates, p=0.031). **c**, Western blot for AHR in cells nucleofected with sg*AHR* and sg*CD8a* control. **d**, ELISA quantification of cytokines from memory CD4$^+$ T cells nucleofected with sg*AHR* or sg*CD8* (n=12 donors). For CXCL13 p=4.88e-4 and IL-22

Author Manuscript Author Manuscript Author Manuscript Author Manuscript

p=4.88e-4. **e**, CXCL13 quantification by ELISA in supernatants of memory $CD4^+$ T cells nucleofected with sg*AHR* or sg*CD8a* in the presence or absence of TGF-β (n=8). From left to right, p=0.0078, 0.0078, 0.0078, 0.0156. **f,g**, Normalized (to DMSO control) ELISA quantification of indicated cytokines in supernatants of memory (**f**) or naive $CD4^+$ T cells (**g**) stimulated under indicated conditions (n=5–7). For AHRinh and TCDD in **f**, respectively, p=7.31e-4 and 0.00304 for CXCL13, and p=0.00159 and 0.0124 for IL-22. For AHRinh and TCDD in **g**, respectively, p=0.0679 and 0.00108 for CXCL13, and p=0.0192 and 0.0157 for IL-22. **h**, Normalized (to DMSO control) ELISA quantification of indicated cytokines in supernatants of memory $CD4^+$ T cells stimulated with AHR agonist FICZ, AHR inhibitor GNF-351, or DMSO control (n=3–4). For FICZ and GNF-351, respectively, p=0.0109 (GNF-351 only) for CXCL13, and p=0.0084 and 0.0393 for IL-22. **i**, Effects of AHR CRISPR deletion (left, n=10) and pharmacological modulation (middle[n=9] and right[n=3]) on IFNγ production measured by ELISA. AHR modulators as in **g** and **h** were tested. Results shown normalized to DMSO control. **j**, Flow cytometry quantification of indicated cytokines in memory CD4+ T cells cultured in polarizing conditions as indicated (n=6). p=0.0316 for IL-17. **k**, ELISA data for CXCL13 (left) and IL-22 (right), normalized to control (DMSO) condition, in supernatants of CD4+ T cells stimulated and cultured with indicated factors. Each dot represents a donor (n=4–5). **l**, ELISA data for $CD8^+$ T cells stimulated in the presence of TGF-β with indicated AHR modulators, normalized to DMSO condition per donor (n=6). For AHRinh and TCDD compared to DMSO, respectively, p=0.0021 and 0.0038 for CXCL13, and p=0.0103 and 0.0032 for IL-22. **m**, ELISA measurement for CXCL13 in supernatants of memory $CD8^+$ T cells nucleofected with sg*AHR* or control CRISPR guide (n=6, P=0.0312). **n**, Expression of ICOS (left) and CD96 (right) by flow cytometry in memory $CD8^+$ T cells stimulated in indicated conditions, normalized to DMSO condition (n=8). For AHRinh and TCDD, respectively, p=0.0158 (AHRinh only) for ICOS, and p=7.09e-3 and 0.0371 for CD96. Data for **f**, **g**, **h, i**, **l** and **n** are shown as mean ± S.D. p-values (NS≥0.05, *p<0.05, **p<0.01, ***p<0.001) by ratio paired t-test for **b**, **f-j**, **l**, **n**, Wilcoxon test in **e, m**.

Author Manuscript Author Manuscript Author Manuscript Author Manuscript

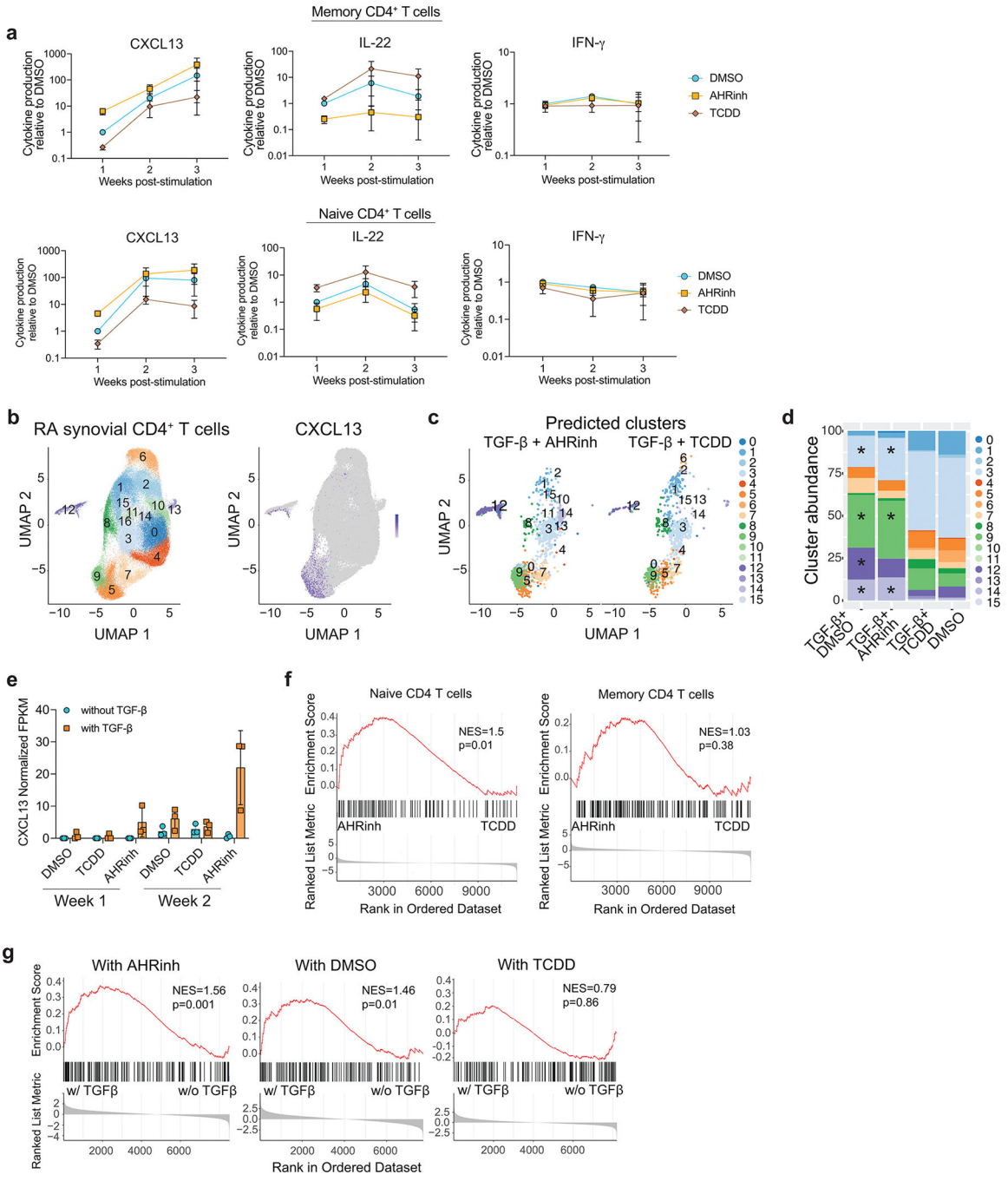

Extended Data Figure 4. Effects of chronic AHR modulation in CD4⁺ T cells.

a, ELISA data for indicated cytokines in supernatants of memory (top) and naïve (bottom) CD4⁺ T cells re-stimulated each week for 3 weeks, normalized to DMSO 1 week result for each donor (n=3–4 donors). **b,** UMAP of RA synovial T cell clusters and expression of CXCL13. **c**, UMAP of cells from Fig. 2e mapped to RA synovial T cell UMAP. **d**, Cluster abundance of *in vitro* cultured memory CD4⁺ T cells from Fig. 2e mapped to RA synovial T cell clusters (n=3). Compared to DMSO condition, from top to bottom, for TGF-β+DMSO p=0.0092, 0.0023, 0.0275, 0.0323, and for TGF-β+AHRinh *P*=0.0188,

Author Manuscript Author Manuscript Author Manuscript Author Manuscript

0.0023, 0.0323. ANOVA with Holm-Sidak test. **e**, CXCL13 expression (by fragments per kilobase of transcript per million mapped reads, FPKM) in bulk RNA-seq samples of cell stimulated under indicated conditions (n=3). **f**, GSEA enrichment plots of Tph gene signature in naïve or memory CD4$^+$ T cells stimulated with TGF-β plus either AHR agonist TCDD or inhibitor (AHRinh) CH-223191. **g**, GSEA enrichment plots for Tph gene signature in T cells stimulated with or without TGF-β, under indicated conditions of AHR agonist TCDD, AHR inhibitor (AHRinh) CH223191, or DMSO control. Mean ± SD shown in **a, e**.

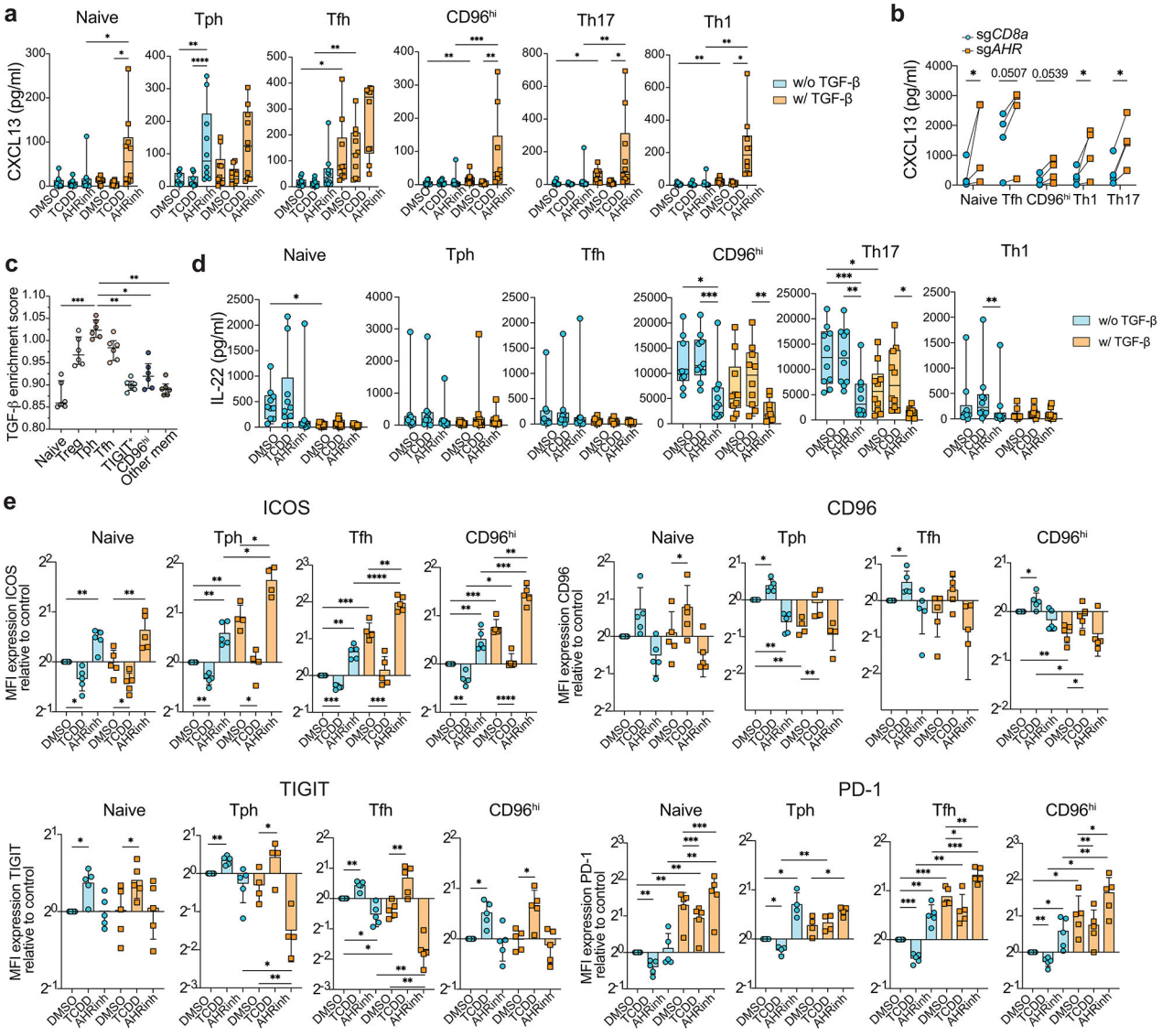

Extended Data Figure 5. Effects of AHR and TGF-β on CD4$^+$ T-cell subsets.

a, ELISA measurement of CXCL13 in supernatants of sorted CD4$^+$ T cell subsets from healthy donors (n=10), stimulated under indicated conditions. Statistical comparisons compare AHR agonist/inhibitor to DMSO within presence or absence of TGF-β, and TGF-β versus no TGF-β within each treatment. p-values from left to right for Naïve: 0.0188, 0.0188, Tph: 0.0032, 4.7e-5, Tfh: 0.0123, 0.0050, CD96hi: 0.0063, 0.0003, 0.0079, Th17:

Author Manuscript Author Manuscript Author Manuscript Author Manuscript

0.0231, 0.0032, 0.0188, Th1: 0.0050, 0.0050, 0.0421. **b**, ELISA measurement of CXCL13 from $CD4^+$ T cell subsets nucleofected with either sg*AHR* or sg*CD8a* CRISPR guides (n=4). From left to right, p=0.0331, 0.0507, 0.0539, 0.0154, 0.0127.**c**, TGF-β gene signature score in bulk RNA-seq data of T cell subsets as in Fig 1h. Comparisons made against Tph subset, from left to right p=1.14e-4, 1.85e-3, 0.0197, 1.85e-3. **d**, ELISA measurement for IL-22 in supernatants of indicated $CD4^+$ T cell subsets stimulated under indicated conditions (n=10). Statistical comparisons performed as in (a). p-values from left to right in each subset is as follows, Naïve: 0.0123, $CD96^{hi}$: 0.0188, 7.24e-4, 1.96e-3, Th17; 4.31e-4, 0.028, 3.17e-3, 0.0188, Th1: 0.002. **e**, Surface expression of indicated markers in $CD4^+$ T cell subsets by flow cytometry, normalized (to DMSO w/o TGF-β) mean fluorescence intensity (MFI), after stimulation as indicated (n=4–5). Statistical comparisons performed as in (a). For ICOS, p-value from left to right in each subset is as follows, Naïve: 0.0188, 8.98e-3, 0.0264, 3.57e-3, Tph: 2.73e-3, 5.21e-3, 5.57e-3, 0.0104, 0.0109, 0.0293, Tfh: 2.20e-4, 1.54e-3, 3.34e-4, 8.89e-4, 5.49e-5, 1.31e-3, $CD96^{hi}$: 5.17e-3, 6.66e-3, 4.52e-4, 0.0154, 2.10e-3, 3.14e-7, 4.39e-3. For CD96, p-value from left to right in each subset is as follows, Naïve: 0.0112, Tph: 0.0312, 0.0205, 6.75e-3, 5.57e-3, Tfh: 0.0315, $CD96^{hi}$: 0.0463, 5.93e-3, 0.0296, 0.0224. For TIGIT, p-value from left to right in each subset is as follows, Naïve: 0.0160, 0.0203, Tph: 2.41e-3, 0.0115, 0.0165, 1.69e-3, Tfh: 3.26e-3, 0.0238, 0.0321, 4.35e-3, 8.51e-3, 6.84e-3, $CD96^{hi}$: 0.0105, 0.0157. For PD-1, p-value from left to right in each subset is as follows, Naïve: 9.17e-3, 4.63e-3, 1.04e-3, 2.33e-3, 8.55e-4, 0.0331, Tph: 0.0133, 0.0119, 3.49e-3, 0.0104, Tfh: 8.49e-4, 5.38e-3, 3.73e-4, 1.03e-3, 1.75e-3, 0.0292, 6.66e-3, $CD96^{hi}$: 9.75e-3, 0.0485, 0.0129, 0.0197, 2.94e-3, 2.07e-3, 0.0328. Boxes indicate median bounded by 1^{st} and 3^{rd} quartile, with bars indicating min/max for **a** and **d**, and as mean ± S.D for **c** and **e**. p-values (*p<0.05, **p<0.01, ***p<0.001, ****p<0.0001) by Friedman's test with post-test by Dunn's test for **a, c** and **d**, and by ratio paired t-test for **b** and **e**.

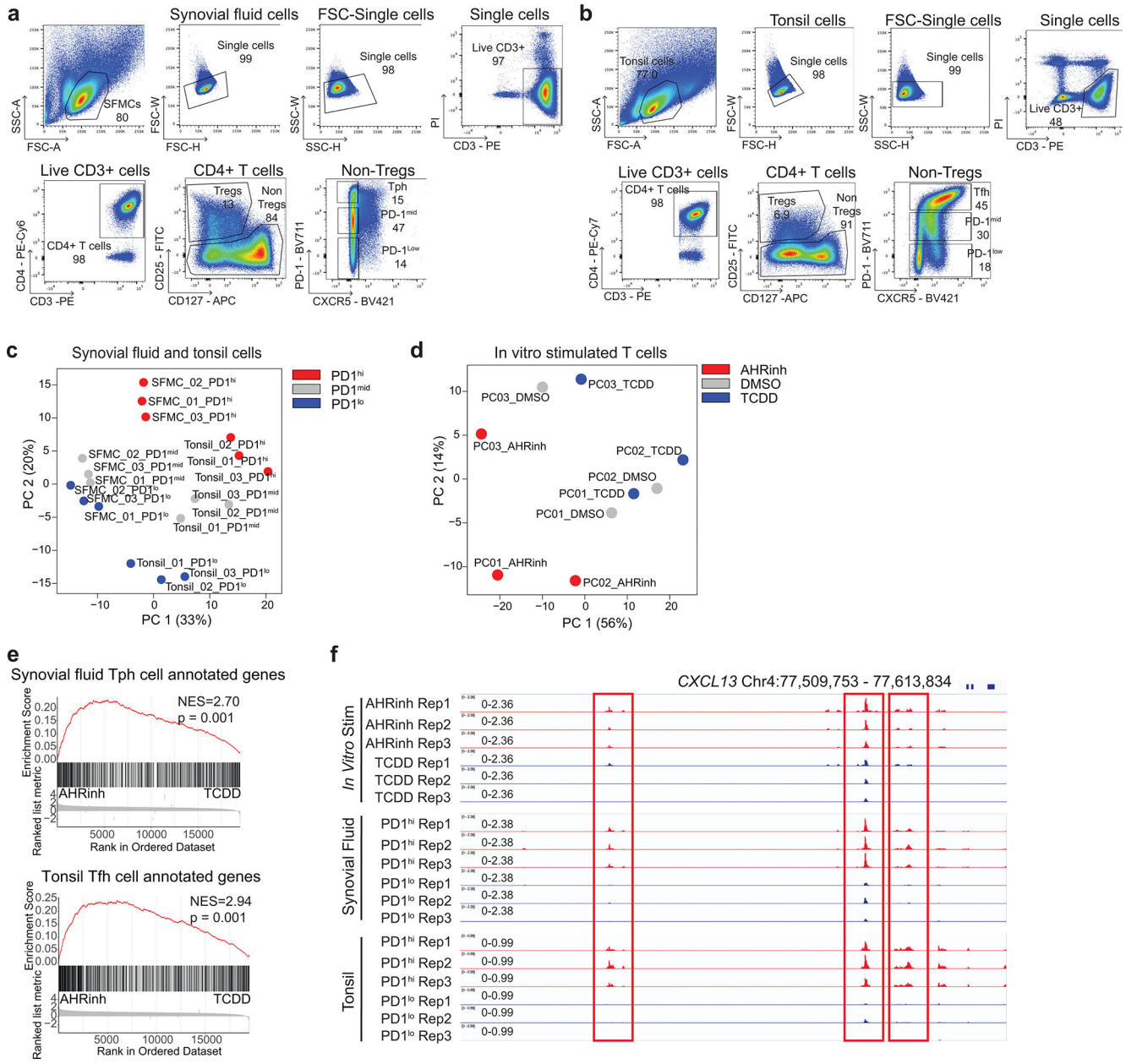

Extended Data Figure 6. ATAC-seq analysis of Tph cells, Tfh cells, and AHR inhibitor-treated cells.

a,**b**, Example flow cytometry cell sorting of CD4$^+$ T cell populations from RA synovial fluid (**a**) or tonsil (**b**) mononuclear cells. **c**, PCA plot of ATAC-seq data from CD4 T cell populations sorted from RA synovial fluid or from tonsil based on PD-1 expression level. **d**, PCA plot of ATAC-seq data from blood CD4$^+$ T cells of healthy donors cultured with DMSO, AHR agonist TCDD or AHR inhibitor (AHRinh) CH-223191 in the presence of TGF-β. **e**, GSEA plots of annotated genes of DARs from synovial fluid Tph cells (top, p=0.001) and tonsil Tfh cells (bottom, p=0.001) in CD4$^+$ T cells treated with AHRinh versus TCDD in presence of TGF-β for 1 week. **f**, Differentially accessible regions (red square)

Author Manuscript Author Manuscript Author Manuscript Author Manuscript

near the *CXCL13* gene locus from ATAC-seq of each indicated cell type/culture condition. TCDD = AHR agonist; AHRinh = AHR inhibitor CH-223191.

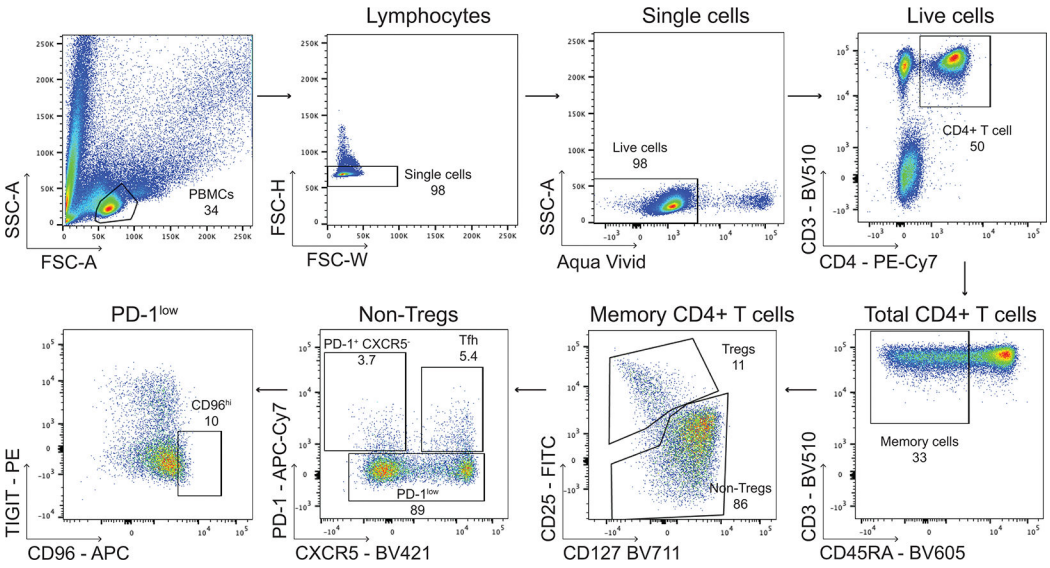

Extended Data Figure 7. Detection of PD-1^{+} Tph cells in SLE PBMC.

Gating strategy for flow cytometry detection of PD-1^{+} CXCR5^{-} Tph cells and CD96^{hi} cells in PBMC from SLE patient after treatment with AHR inhibitor (AHRinh) CH-223191.

Author Manuscript Author Manuscript Author Manuscript Author Manuscript

Author Manuscript Author Manuscript Author Manuscript Author Manuscript

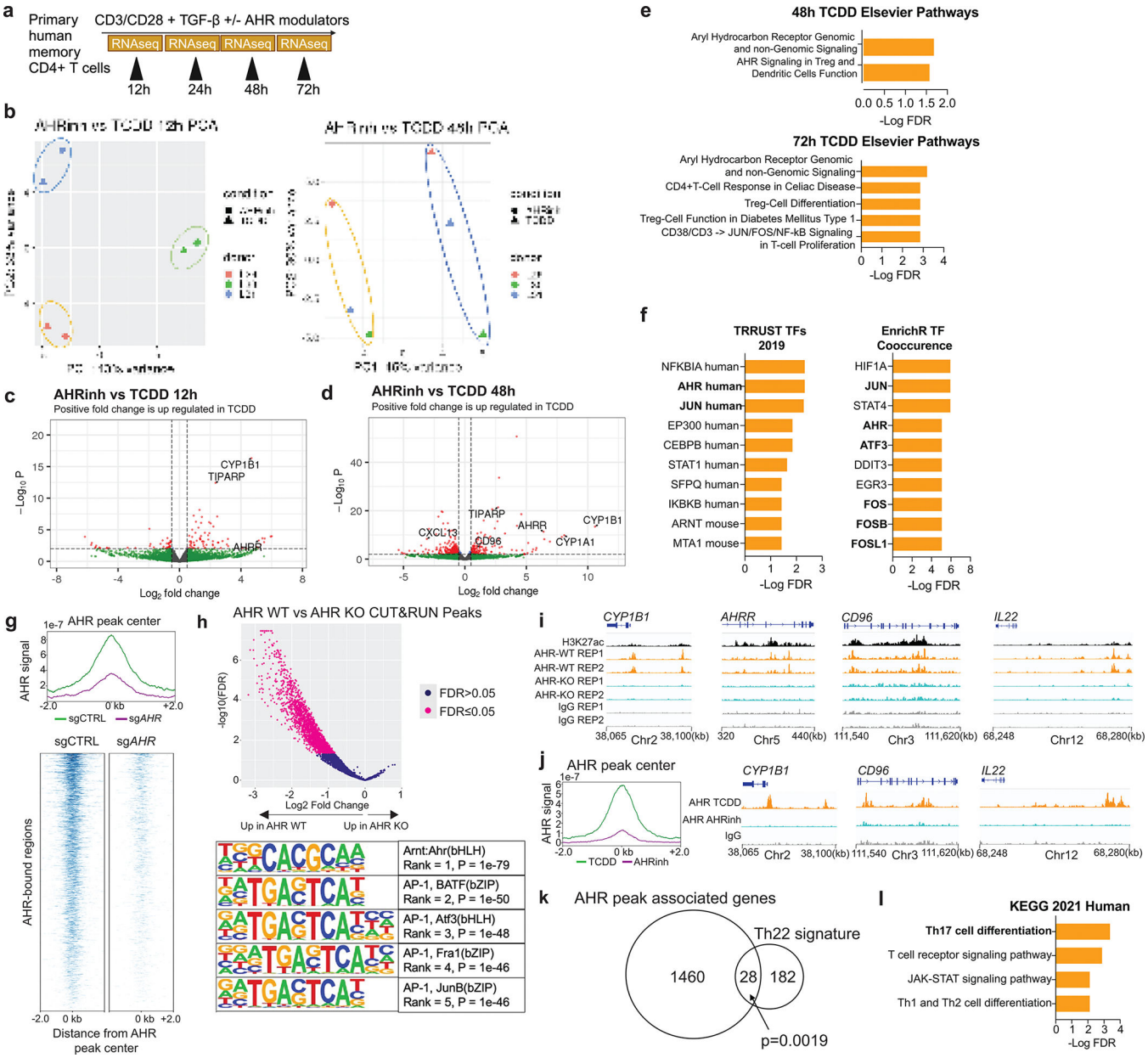

Extended Data Figure 8. Transcriptomic and epigenetic evaluation of AHR activation in T cells and association with AP-1 family members.

a, Schematic of RNA-Seq time course experiment to identify early transcriptomic events of AHR modulation. **b**, PCA plots of RNA-seq samples after 12 hours (left) and 48 hours (right) of stimulation with TGF-β and either AHR agonist (TCDD) or AHR inhibitor (AHRinh) CH-223191. **c**,**d**, Volcano plots of DESeq2 results from RNA-Seq analysis of memory CD4$^+$ T cells cultured for 12 hours (**c**) and 48 hours (**d**) in TGF-β and either TCDD or AHRinh. The samples used for DESeq2 analysis correspond with the PCA plots in **b**. **e**, Pathway enrichment analysis of genes upregulated in TCDD-treated CD4$^+$ T cells at 48 and 72 hours of culture, based on Elsevier pathway collection. **f**, Transcription factor enrichment analysis of samples at 12 hours using EnrichR databases TRRUST

Transcription factors 2019 (left) and EnrichR Transcription factor Co-occurence (right). **g**, AHR CUT&RUN binding signal (top) and heat map (bottom). **h**, Volcano plot of AHR CUT&RUN Diffbind analysis comparing samples with and without AHR CRISPR knockout (top) and HOMER motif analysis of all upregulated peaks found in AHR WT samples (bottom). **i**, Representative AHR binding regions. **j**, Comparison of AHR binding in cells treated with AHR agonist or AHR antagonist. **k**, Venn diagram of overlapped genes bound by AHR with Th22 signature genes as shown in Fig 1e, hypergeometric *P*-value is shown. **l**, Pathway enrichment analysis of AHR-bound peak associated genes. TCDD = AHR agonist; AHRinh = AHR inhibitor, CH-223191.

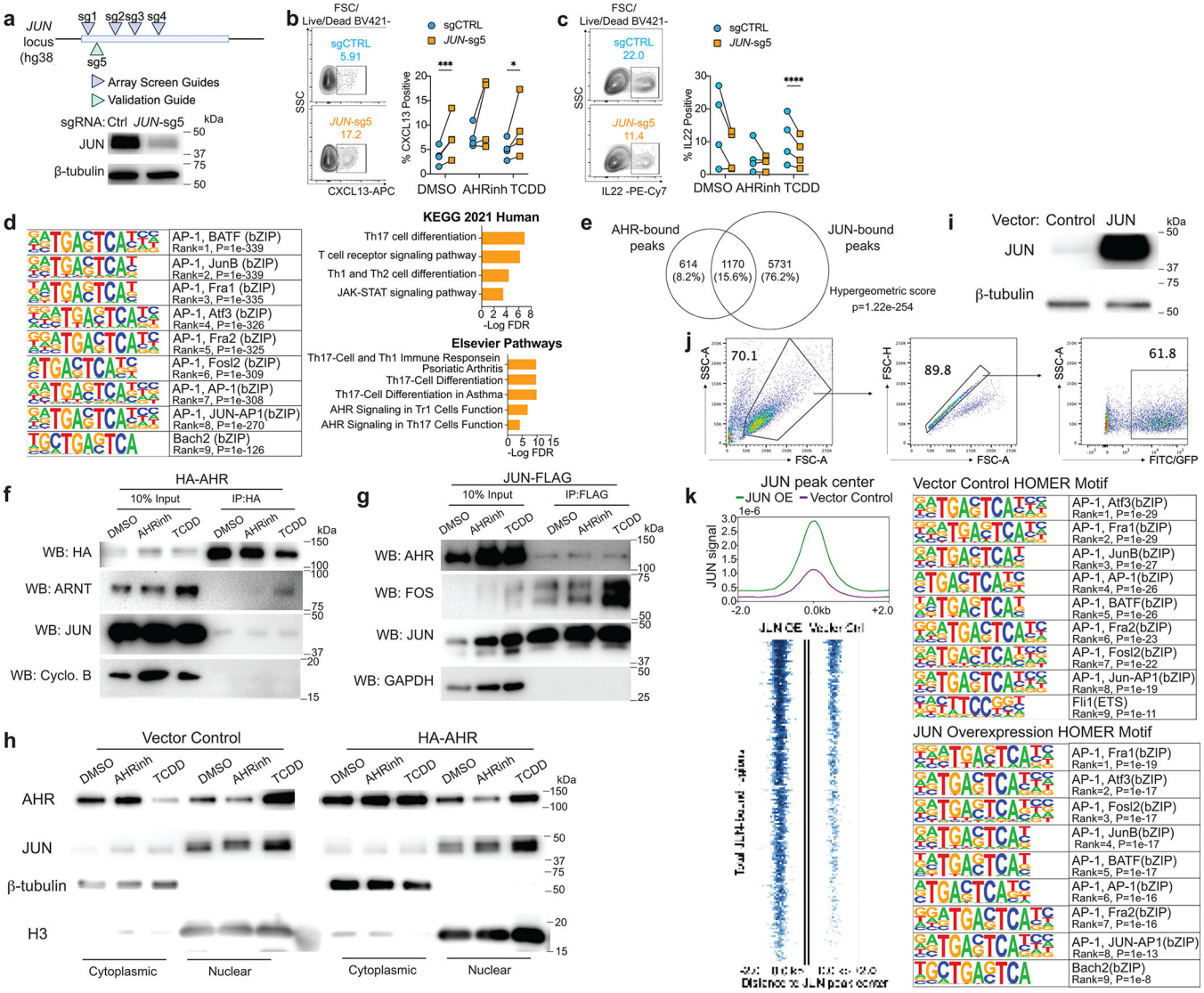

Extended Data Fig 9. Overexpression of JUN in human CD4$^+$ T cells.

a, Illustration of JUN-targeting sgRNAs used in CRISPR screens and validation experiments, and Western blot detection of JUN in T cells nucleofected with control (sgCtrl) or JUN-targeting guide (*JUN*-sg5), western blot has been reproduced in at least 5 different biological donors. **b**, Flow cytometry detection of CXCL13 in memory CD4$^+$

Author Manuscript Author Manuscript Author Manuscript Author Manuscript

Author Manuscript Author Manuscript Author Manuscript Author Manuscript

T cells nucleofected with control (upper left) or *JUN*-sg5 (lower left), and quantification after stimulation under indicated conditions (n=4, right), p-value from left to right: 3.81e-4, 0.0372. **c**, Flow cytometry detection of IL-22 detection and quantification of IL-22 as for CXCL13 in **b**. For flow cytometry data (right, n=4, p=3.6e-5). **d**, Top 10 HOMER motifs (left) from JUN CUT&RUN peaks in TCDD-treated memory $CD4^+$ T cells with pathway enrichment analysis (middle and right). **e**, Venn diagram of CUT&RUN peaks bound by AHR and JUN. **f**,**g** Verification of AHR and JUN as interactors. Immunoblot (WB) analysis of HA (**f**) or Flag (**g**) immunoprecipitates from the indicated cell lysates probed with the indicated antibodies, both have been repeated two times in HEK293T cells. **h**, Cytoplasmic or nuclear extracts (as indicated on bottom) from HEK293T cells stably expressing HA-AHR or vector control treated with AHRinh, TCDD or vehicle control (DMSO) were immunoblotted for AHR, JUN and respective controls (β-tubulin for cytoplasmic extract, Histone H3 for nuclear extract), this has been repeated 3 times in HEK293T cells. **i**, JUN expression by Western blot in T cells transduced with JUN overexpression construct or control vector. **j**, Example of flow cytometry sorting to obtain JUN-overexpressing cells based on GFP positivity. **k**, JUN overexpression (JUN OE) CUT&RUN assessment by peak density on total JUN bound peaks compared to vector control as in Fig 3k and top HOMER motifs for each respective condition. p-values (*p<0.05, **p<0.01, ***p<0.001, ****p<0.0001) by ratio paired t-test for **b** and **c**. TCDD = AHR agonist; AHRinh = AHR inhibitor, CH-223191.

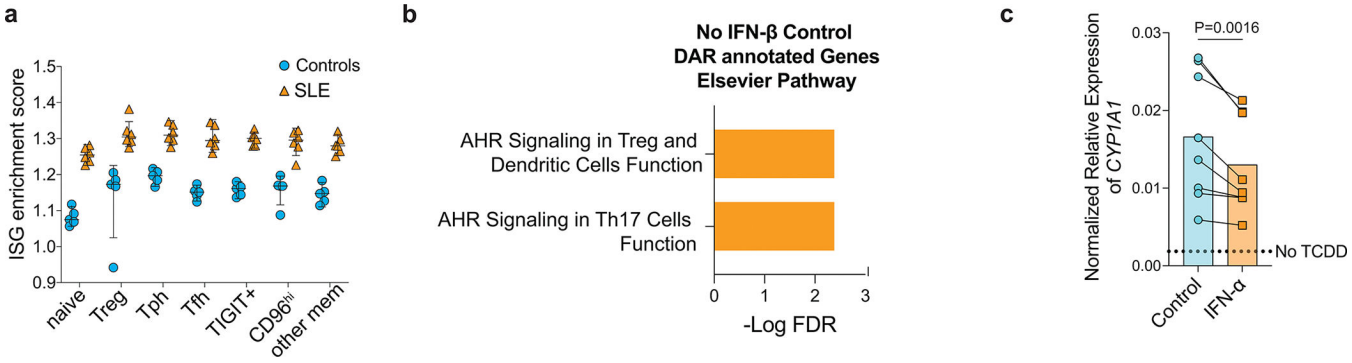

Extended Data Fig 10. Increased IFN in SLE patients inhibit AHR signaling.

a, IFN signature score in RNA-seq data of $CD4^+$ T cell subsets from SLE and control patients as in Fig 1g. Median ± interquartile range shown. b, Elsevier pathway enrichment from annotated genes of DAR in No IFN-β control treated $CD4^+$ T cells. **c**, Normalized relative expression of *CYP1A1* measured by qPCR in $CD4^+$ T cells cultured in DMSO or TCDD with the addition of vehicle control or IFN-α (n=8, p=0.0016 by paired t-test). TCDD = AHR agonist.

Supplementary Material

Refer to Web version on PubMed Central for supplementary material.

Author Manuscript Author Manuscript Author Manuscript Author Manuscript

Acknowledgements

We thank the Accelerating Medicines Partnership RA/SLE Network for generation of the RA synovial scRNA-Seq data. This work has been supported in part by funding from the Burroughs Wellcome Fund Career Award in Medical Sciences, NIAMS K08 AR072791, P30 AR070253, Lupus Research Alliance Target Identification in Lupus award, Rheumatology Research Foundation K Supplement, and NIAMS R01 AR078769 (to DAR and JC); NIAMS R01 (to MBB); and NIAID R01 AI176599, P30 AI117943, R01 AI165236, and U54 AI170792 (to JFH). CL was supported by an NCI F31 fellowship (F31CA268839). VSW was supported by a Lupus Research Alliance Postdoctoral Award. Support for mass cytometry data was provided by Merck Sharpe & Dohme. Support for scRNA-Seq of in vitro stimulated T cells was provided by Janssen Research & Development, LLC. We thank the BWH Center for Cellular Profiling for cell sorting and scRNA-seq data generation and Gary Perdew for providing the AHR luciferase reporter cell line. This work was supported by the Northwestern University – Flow Cytometry Core Facility supported by Cancer Center Support Grant (NCI CA060553). Research reported in this publication was supported by Northwestern University Skin Biology & Diseases Resource-Based center of the National Institutes of Health under award number P30AR075049. We also thank Admera Health LLC for their contribution to sequencing efforts.

Data Availability

Bulk RNA-Seq data of sorted T cell subsets and long-term in vitro stimulated cells, scRNA-Seq of in vitro stimulated cells, scRNA-seq of T cells before and after anifrolumab treatment, and ATAC-Seq data on in vitro stimulated cells, synovial fluid cells, and tonsils are available through dbGAP as study phs003582.v1.p1. CUT&RUN sequencing data and bulk RNA-seq timecourse of in vitro stimulation are available under accession no. GSE233050. scRNA-seq data of RA synovial T cells were obtained from Synapse (https://doi.org:10.7303/syn52297840)[20]. Bulk RNA-seq and ATAC-seq data of IFN-treated cells were obtained from GSE195543[29]. Source data are provided with this paper.

Accelerating Medicines Partnership: RA/SLE Network

Jennifer Albrecht[15], Jennifer H. Anolik[15], William Apruzzese[16], Jennifer L. Barnas[15], Joan M. Bathon[17], Ami Ben-Artzi[18], Brendan F. Boyce[19], David L. Boyle[20], Michael B. Brenner[4], S. Louis Bridges Jr.[21,22], Vivian P. Bykerk[21,22], Debbie Campbell[15], Arnold Ceponis[20], Adam Chicoine[4], Michelle Curtis[4,33,34,35,36], Kevin D. Deane[23], Edward DiCarlo[24], Laura T. Donlin[21,22], Patrick Dunn[25,26], Andrew Filer[27,28,29], Hayley Carr[27,29], Gary S. Firestein[19], Lindsy Forbess[18], Laura Geraldino-Pardilla[17], Susan M. Goodman[21,22], Ellen M. Gravallese[4], Peter K. Gregersen[30], Joel M. Guthridge[31], Maria Gutierrez-Arcelus[32,33,34,35,36], V. Michael Holers[23], Diane Horowitz[30], Laura B. Hughes[37], Lionel B. Ivashkiv[21,22], Kazuyoshi Ishigaki[38], Judith A. James[31], A. Helena Jonsson[23], Joyce B. Kang[4,33,34,35,36], Gregory Keras[4], Ilya Korsunsky[4,33,34,35,36], Amit Lakhanpal[21,22], James A. Lederer[39], Miles J. Lewis[40,41], Yuhong Li[4], Katherine Liao[4], Arthur M. Mandelin II[42], Ian Mantel[21,22], Kathryne E. Marks[4], Mark Maybury[27,29], Andrew McDavid[43], Mandy J. McGeachy[44], Joseph R. Mears[4,33,34,35,36], Nida Meednu[15], Nghia Millard[4,33,34,35,36], Larry Moreland[23], Saba Nayar[27,28], Alessandra Nerviani[45,46], Dana E. Orange[21], Harris Perlman[42], Costantino Pitzalis[45,46,47], Javier Rangel-Moreno[15], Soumya Raychaudhuri[4,33,34,35,36], Karim Raza[27,29], Yakir Reshef[4,33,34,35,36], Christopher Ritchlin[15], Felice Rivellese[45,46], William H. Robinson[48], Laurie Rumker[4,33,34,35,36], Ilfita Sahbudin[27,29], Saori Sakaue[4,33,34,35,36], Jennifer A. Seifert[23], Dagmar Scheel-Toellner[27,29], Anvita Singaraju[21,22], Kamil Slowikowski[4,33,34,35,36], Melanie Smith[21], Darren Tabechian[15], Paul J. Utz[48], Gerald F. M. Watts[4], Kevin Wei[4], Kathryn

Author Manuscript Author Manuscript Author Manuscript Author Manuscript

Weinand[4,33,34,35,36], Dana Weisenfeld[4], Michael Weisman[18], Qian Xiao[4,33,34,35,36], Fan Zhang[49], Zhu Zhu[4], Andrew Cordle[50,] Aaron Wyse[50]

[15]Division of Allergy, Immunology and Rheumatology, Department of Medicine, University of Rochester Medical Center, Rochester, NY, USA

[16]Accelerating Medicines Partnership: RA/SLE Network, Bethesda, MD, USA

[17]Division of Rheumatology, Columbia University College of Physicians and Surgeons, New

York, NY, USA.

[18]Division of Rheumatology, Cedars-Sinai Medical Center, Los Angeles, CA, USA.

University of California, San Diego, La Jolla, CA, USA.

[19]Department of Pathology and Laboratory Medicine, University of Rochester Medical Center, Rochester, NY,

[20]Division of Rheumatology, Allergy and Immunology, University of California, San Diego, La Jolla, CA, USA.

[21]Hospital for Special Surgery, New York, NY, USA.

[22]Weill Cornell Medicine, New York, NY, USA.

[23]Division of Rheumatology, University of Colorado School of Medicine, Aurora, CO, USA

[24]Department of Pathology and Laboratory Medicine, Hospital for Special Surgery, New York, NY, USA.

[25]Division of Allergy, Immunology and Transplantation, National Institute of Allergy and Infectious Diseases, National Institutes of Health, Bethesda, MD, USA.

[26]Northrop Grumman Health Solutions, Rockville, MD, USA.

[27]Rheumatology Research Group, Institute for Inflammation and Ageing, University of Birmingham, Birmingham, UK.

[28]Birmingham Tissue Analytics, Institute of Translational Medicine, University of Birmingham, Birmingham, UK.

[29]NIHR Birmingham Biomedical Research Center and Clinical Research Facility, University of Birmingham, Queen Elizabeth Hospital, Birmingham, UK.

[30]Feinstein Institute for Medical Research, Northwell Health, Manhasset, New York, NY, USA.

Author Manuscript Author Manuscript Author Manuscript Author Manuscript

[31]Department of Arthritis and Clinical Immunology, Oklahoma Medical Research Foundation, Oklahoma City, OK, USA.

[32]Division of Immunology, Department of Pediatrics, Boston Children's Hospital and Harvard Medical School, Boston, MA, USA.

[33]Center for Data Sciences, Brigham and Women's Hospital, Boston, MA, USA.

[34]Division of Genetics, Department of Medicine, Brigham and Women's Hospital and Harvard Medical School, Boston, MA, USA.

[35]Department of Biomedical Informatics, Harvard Medical School, Boston, MA, USA.

[36]Broad Institute of MIT and Harvard, Cambridge, MA, USA.

[37]Division of Clinical Immunology and Rheumatology, Department of Medicine, University of Alabama at Birmingham, Birmingham, AL, USA.

[38]Laboratory for Human Immunogenetics, RIKEN Center for Integrative Medical Sciences, Yokohama, Japan.

[39]Department of Surgery, Brigham and Women's Hospital and Harvard Medical School, Boston, MA, USA

[40]Centre for Experimental Medicine and Rheumatology, EULAR Centre of Excellence, William Harvey Research Institute, Queen Mary University of London, London, UK.

[41]Barts Health NHS Trust, Barts Biomedical Research Centre (BRC), National Institute for Health and Care Research (NIHR), London, UK.

[42]Division of Rheumatology, Department of Medicine, Northwestern University Feinberg School of Medicine, Chicago, IL, USA

[43]Department of Biostatistics and Computational Biology, University of Rochester School of Medicine and Dentistry, Rochester, NY, USA.

[44]Division of Rheumatology and Clinical Immunology, University of Pittsburgh School of Medicine, Pittsburgh, PA, USA

[45]Centre for Experimental Medicine and Rheumatology, EULAR Centre of Excellence, William Harvey Research Institute, Queen Mary University of London, London, UK.

[46]Barts Health NHS Trust, Barts Biomedical Research Centre (BRC), National Institute for Health and Care Research (NIHR), London, UK.

[47]Department of Biomedical Sciences, Humanitas University and Humanitas Research Hospital, Milan, Italy

[48]Division of Immunology and Rheumatology, Institute for Immunity, Transplantation and Infection, Stanford University School of Medicine, Stanford, CA, USA.

Author Manuscript Author Manuscript Author Manuscript Author Manuscript

[49]Division of Rheumatology and the Center for Health Artificial Intelligence, University of Colorado School of Medicine, Aurora, CO, USA

[50]Department of Radiology, University of Pittsburgh Medical Center, Pittsburgh, PA, USA

References

1. Tsokos GC Autoimmunity and organ damage in systemic lupus erythematosus. Nature immunology 21, 605–614 (2020). 10.1038/s41590-020-0677-6 [PubMed: 32367037]
2. Jenks SA, Cashman KS, Woodruff MC, Lee FE & Sanz I Extrafollicular responses in humans and SLE. Immunological reviews 288, 136–148 (2019). 10.1111/imr.12741 [PubMed: 30874345]
3. Bocharnikov AV et al. PD-1hi CXCR5- T peripheral helper cells promote B cells responses in lupus via MAF and IL-21. JCI insight (2019). 10.1172/jci.insight.130062
4. He J et al. Circulating precursor CCR7(lo)PD-1(hi) CXCR5(+) CD4(+) T cells indicate Tfh cell activity and promote antibody responses upon antigen reexposure. Immunity 39, 770–781 (2013). 10.1016/j.immuni.2013.09.007 [PubMed: 24138884]
5. Havenar-Daughton C et al. CXCL13 is a plasma biomarker of germinal center activity. Proc Natl Acad Sci U S A 113, 2702–2707 (2016). 10.1073/pnas.1520112113 [PubMed: 26908875]
6. Rao DA et al. Pathologically expanded peripheral T helper cell subset drives B cells in rheumatoid arthritis. Nature 542, 110–114 (2017). 10.1038/nature20810 [PubMed: 28150777]
7. Morand EF et al. Trial of Anifrolumab in Active Systemic Lupus Erythematosus. The New England journal of medicine 382, 211–221 (2020). 10.1056/NEJMoa1912196 [PubMed: 31851795]
8. Choi JY et al. Circulating follicular helper-like T cells in systemic lupus erythematosus: association with disease activity. Arthritis & rheumatology 67, 988–999 (2015). 10.1002/art.39020 [PubMed: 25581113]
9. Jenks SA et al. Distinct Effector B Cells Induced by Unregulated Toll-like Receptor 7 Contribute to Pathogenic Responses in Systemic Lupus Erythematosus. Immunity 49, 725–739 e726 (2018). 10.1016/j.immuni.2018.08.015 [PubMed: 30314758]
10. Wang S et al. IL-21 drives expansion and plasma cell differentiation of autoreactive CD11c(hi)T-bet(+) B cells in SLE. Nature communications 9, 1758 (2018). 10.1038/s41467-018-03750-7
11. Crotty S Follicular helper CD4 T cells (TFH). Annual review of immunology 29, 621–663 (2011). 10.1146/annurev-immunol-031210-101400
12. Gunn MD et al. A B-cell-homing chemokine made in lymphoid follicles activates Burkitt's lymphoma receptor-1. Nature 391, 799–803 (1998). 10.1038/35876 [PubMed: 9486651]
13. Kobayashi S et al. TGF-beta induces the differentiation of human CXCL13-producing CD4(+) T cells. Eur J Immunol 46, 360–371 (2016). 10.1002/eji.201546043 [PubMed: 26541894]
14. Yoshitomi H et al. Human Sox4 facilitates the development of CXCL13-producing helper T cells in inflammatory environments. Nature communications 9, 3762 (2018). 10.1038/s41467-018-06187-0
15. Reshef YA et al. Co-varying neighborhood analysis identifies cell populations associated with phenotypes of interest from single-cell transcriptomics. Nature biotechnology 40, 355–363 (2022). 10.1038/s41587-021-01066-4
16. Trifari S, Kaplan CD, Tran EH, Crellin NK & Spits H Identification of a human helper T cell population that has abundant production of interleukin 22 and is distinct from T(H)-17, T(H)1 and T(H)2 cells. Nat Immunol 10, 864–871 (2009). 10.1038/ni.1770 [PubMed: 19578368]
17. Eyerich K, Dimartino V & Cavani A IL-17 and IL-22 in immunity: Driving protection and pathology. Eur J Immunol 47, 607–614 (2017). 10.1002/eji.201646723 [PubMed: 28295238]
18. Veldhoen M et al. The aryl hydrocarbon receptor links TH17-cell-mediated autoimmunity to environmental toxins. Nature 453, 106–109 (2008). 10.1038/nature06881 [PubMed: 18362914]
19. Ramirez JM et al. Activation of the aryl hydrocarbon receptor reveals distinct requirements for IL-22 and IL-17 production by human T helper cells. Eur J Immunol 40, 2450–2459 (2010). 10.1002/eji.201040461 [PubMed: 20706985]

Author Manuscript Author Manuscript Author Manuscript Author Manuscript

20. Zhang F et al. Deconstruction of rheumatoid arthritis synovium defines inflammatory subtypes. Nature 623, 616–624 (2023). 10.1038/s41586-023-06708-y [PubMed: 37938773]
21. Love MI, Huber W & Anders S Moderated estimation of fold change and dispersion for RNA-seq data with DESeq2. Genome Biol 15, 550 (2014). 10.1186/s13059-014-0550-8 [PubMed: 25516281]
22. Long WP, Pray-Grant M, Tsai JC & Perdew GH Protein kinase C activity is required for aryl hydrocarbon receptor pathway-mediated signal transduction. Molecular pharmacology 53, 691–700 (1998). 10.1124/mol.53.4.691 [PubMed: 9547360]
23. MacPherson L et al. Aryl hydrocarbon receptor repressor and TiPARP (ARTD14) use similar, but also distinct mechanisms to repress aryl hydrocarbon receptor signaling. Int J Mol Sci 15, 7939–7957 (2014). 10.3390/ijms15057939 [PubMed: 24806346]
24. Gutierrez-Vazquez C & Quintana FJ Regulation of the Immune Response by the Aryl Hydrocarbon Receptor. Immunity 48, 19–33 (2018). 10.1016/j.immuni.2017.12.012 [PubMed: 29343438]
25. Rothhammer V & Quintana FJ The aryl hydrocarbon receptor: an environmental sensor integrating immune responses in health and disease. Nat Rev Immunol 19, 184–197 (2019). 10.1038/s41577-019-0125-8 [PubMed: 30718831]
26. Bennett L et al. Interferon and granulopoiesis signatures in systemic lupus erythematosus blood. J Exp Med 197, 711–723 (2003). 10.1084/jem.20021553 [PubMed: 12642603]
27. Panwar B et al. Multi-cell type gene coexpression network analysis reveals coordinated interferon response and cross-cell type correlations in systemic lupus erythematosus. Genome Res 31, 659–676 (2021). 10.1101/gr.265249.120 [PubMed: 33674349]
28. Furie RA et al. Type I interferon inhibitor anifrolumab in active systemic lupus erythematosus (TULIP-1): a randomised, controlled, phase 3 trial. The Lancet Rheumatology 1, e208–e219 (2019). 10.1016/S2665-9913(19)30076-1 [PubMed: 38229377]
29. Sumida TS et al. Type I interferon transcriptional network regulates expression of coinhibitory receptors in human T cells. Nat Immunol 23, 632–642 (2022). 10.1038/s41590-022-01152-y [PubMed: 35301508]
30. Frank DA, Robertson MJ, Bonni A, Ritz J & Greenberg ME Interleukin 2 signaling involves the phosphorylation of Stat proteins. Proc Natl Acad Sci U S A 92, 7779–7783 (1995). 10.1073/pnas.92.17.7779 [PubMed: 7544001]
31. Zella D et al. IFN-alpha 2b reduces IL-2 production and IL-2 receptor function in primary CD4+ T cells. J Immunol 164, 2296–2302 (2000). 10.4049/jimmunol.164.5.2296 [PubMed: 10679063]
32. Rothhammer V et al. Type I interferons and microbial metabolites of tryptophan modulate astrocyte activity and central nervous system inflammation via the aryl hydrocarbon receptor. Nat Med 22, 586–597 (2016). 10.1038/nm.4106 [PubMed: 27158906]
33. Shinde R et al. Apoptotic cell-induced AhR activity is required for immunological tolerance and suppression of systemic lupus erythematosus in mice and humans. Nat Immunol 19, 571–582 (2018). 10.1038/s41590-018-0107-1 [PubMed: 29760532]
34. Hatzi K et al. BCL6 orchestrates Tfh cell differentiation via multiple distinct mechanisms. J Exp Med 212, 539–553 (2015). 10.1084/jem.20141380 [PubMed: 25824819]
35. Seth A et al. AP-1-independent NFAT signaling maintains follicular T cell function in infection and autoimmunity. J Exp Med 220 (2023). 10.1084/jem.20211110
36. Park J et al. Integrated genomic analyses of cutaneous T-cell lymphomas reveal the molecular bases for disease heterogeneity. Blood 138, 1225–1236 (2021). 10.1182/blood.2020009655 [PubMed: 34115827]
37. Liu B, Zhang Y, Wang D, Hu X & Zhang Z Single-cell meta-analyses reveal responses of tumor-reactive CXCL13(+) T cells to immune-checkpoint blockade. Nat Cancer 3, 1123–1136 (2022). 10.1038/s43018-022-00433-7 [PubMed: 36138134]
38. Lowery FJ et al. Molecular signatures of antitumor neoantigen-reactive T cells from metastatic human cancers. Science 375, 877–884 (2022). 10.1126/science.abl5447 [PubMed: 35113651]
39. Lynn RC et al. c-Jun overexpression in CAR T cells induces exhaustion resistance. Nature 576, 293–300 (2019). 10.1038/s41586-019-1805-z [PubMed: 31802004]

Author Manuscript Author Manuscript Author Manuscript Author Manuscript

40. Liu Y et al. IL-2 regulates tumor-reactive CD8(+) T cell exhaustion by activating the aryl hydrocarbon receptor. Nat Immunol 22, 358–369 (2021). 10.1038/s41590-020-00850-9 [PubMed: 33432230]
41. Luther SA, Lopez T, Bai W, Hanahan D & Cyster JG BLC expression in pancreatic islets causes B cell recruitment and lymphotoxin-dependent lymphoid neogenesis. Immunity 12, 471–481 (2000). 10.1016/s1074-7613(00)80199-5 [PubMed: 10843380]
42. Botia-Sanchez M et al. Gut epithelial barrier dysfunction in lupus triggers a differential humoral response against gut commensals. Front Immunol 14, 1200769 (2023). 10.3389/fimmu.2023.1200769 [PubMed: 37346043]
43. Manfredo Vieira S et al. Translocation of a gut pathobiont drives autoimmunity in mice and humans. Science 359, 1156–1161 (2018). 10.1126/science.aar7201 [PubMed: 29590047]
44. Arshad T, Mansur F, Palek R, Manzoor S & Liska V A Double Edged Sword Role of Interleukin-22 in Wound Healing and Tissue Regeneration. Front Immunol 11, 2148 (2020). 10.3389/fimmu.2020.02148 [PubMed: 33042126]
45. Aringer M et al. 2019 European League Against Rheumatism/American College of Rheumatology Classification Criteria for Systemic Lupus Erythematosus. Arthritis Rheumatol 71, 1400–1412, doi:10.1002/art.40930 (2019). [PubMed: 31385462]
46. Nowicka M et al. CyTOF workflow: differential discovery in high-throughput high-dimensional cytometry datasets. F1000Res 6, 748, doi:10.12688/f1000research.11622.3 (2017). [PubMed: 28663787]
47. Fonseka CY et al. Mixed-effects association of single cells identifies an expanded effector CD4(+) T cell subset in rheumatoid arthritis. Science translational medicine 10, doi:10.1126/scitranslmed.aaq0305 (2018).
48. Hultquist JF et al. CRISPR-Cas9 genome engineering of primary CD4(+) T cells for the interrogation of HIV-host factor interactions. Nature protocols 14, 1–27, doi:10.1038/s41596-018-0069-7 (2019). [PubMed: 30559373]
49. Doench JG et al. Optimized sgRNA design to maximize activity and minimize off-target effects of CRISPR-Cas9. Nature Biotechnology 34, 184–191, doi:10.1038/nbt.3437 (2016).
50. Meers MP, Tenenbaum D & Henikoff S Peak calling by Sparse Enrichment Analysis for CUT&RUN chromatin profiling. Epigenetics Chromatin 12, 42, doi:10.1186/s13072-019-0287-4 (2019). [PubMed: 31300027]
51. Yu G, Wang LG & He QY ChIPseeker: an R/Bioconductor package for ChIP peak annotation, comparison and visualization. Bioinformatics 31, 2382–2383, doi:10.1093/bioinformatics/btv145 (2015). [PubMed: 25765347]
52. Conesa A, Nueda MJ, Ferrer A & Talon M maSigPro: a method to identify significantly differential expression profiles in time-course microarray experiments. Bioinformatics 22, 1096–1102, doi:10.1093/bioinformatics/btl056 (2006). [PubMed: 16481333]
53. Kang JB et al. Efficient and precise single-cell reference atlas mapping with Symphony. Nature communications 12, 5890, doi:10.1038/s41467-021-25957-x (2021).
54. Zhang F et al. Defining inflammatory cell states in rheumatoid arthritis joint synovial tissues by integrating single-cell transcriptomics and mass cytometry. Nature immunology 20, 928–942, doi:10.1038/s41590-019-0378-1 (2019). [PubMed: 31061532]
55. Hollbacher B et al. Transcriptomic Profiling of Human Effector and Regulatory T Cell Subsets Identifies Predictive Population Signatures. Immunohorizons 4, 585–596, doi:10.4049/immunohorizons.2000037 (2020). [PubMed: 33037096]
56. Morand EF et al. Trial of Anifrolumab in Active Systemic Lupus Erythematosus. N Engl J Med 382, 211–221, doi:10.1056/NEJMoa1912196 (2020). [PubMed: 31851795]

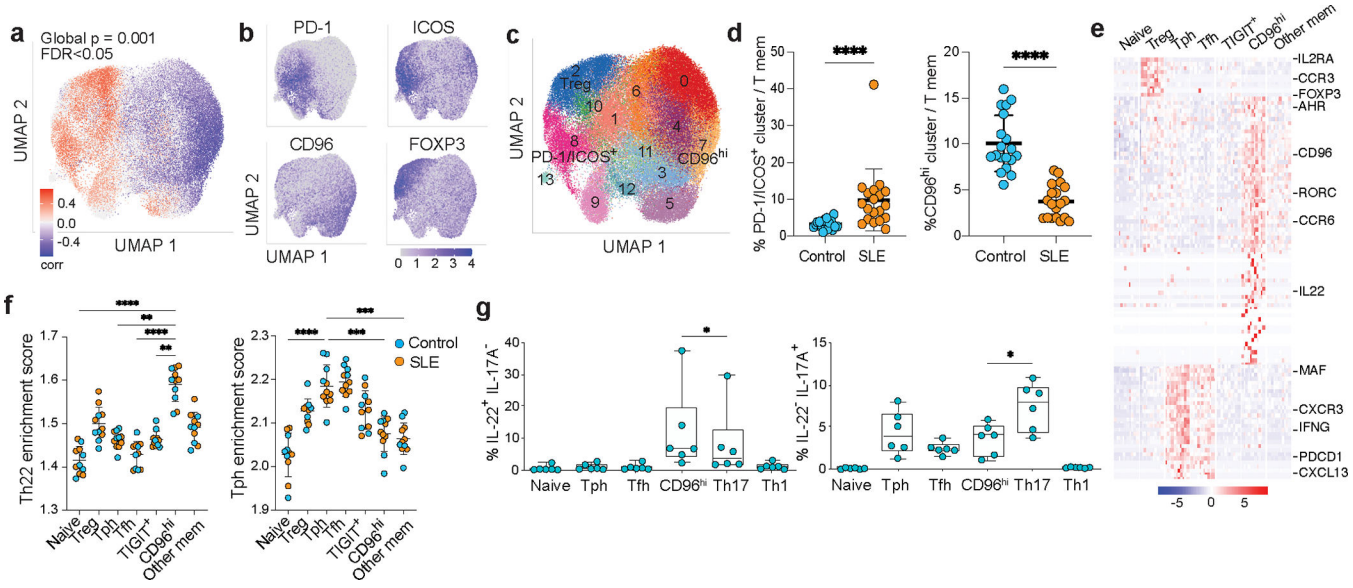

Figure 1. Imbalanced CXCL13^{+} Tph/Tfh cells versus IL-22^{+} CD96^{hi} cells in SLE patients.

a, UMAP showing co-varying neighborhood analysis (red, enriched in SLE; blue, enriched in controls by FDR<0.05, global p=0.001). **b**, Feature plots showing expression of indicated proteins on memory CD4^{+} T cells. **c**, UMAP showing memory CD4^{+} T cell clusters. **d**, Quantification of indicated clusters in SLE patients (n=19) and controls (n=19), p=6.3e-6 for PD-1/ICOS^{+}, p=2.9e-9 for CD96^{hi}. **e**, Heatmap of upregulated genes in Treg, Tph/Tfh cells, and CD96^{hi} cells in RNA-seq data from blood T cell subsets (n=11; 6 SLE patients, 5 controls). **f**, Th22 and Tph gene signature scores in RNA-seq data in **e**. Th22 score compared to CD96^{hi} T cells, p-values from left to right: 6.24e-8, 9.53e-3, 1.11e-7, 4.75e-3. Tph score compared to Tph cells, from left to right p= 3.42e-7, 4.73e-4, 2.04e-4. **g**, Flow cytometry quantification of IL-22 and IL-17A cells in cell subsets from controls (n=6). Boxes indicate median bounded by 1st and 3rd quartile; bars indicate min/max. Comparing between CD96^{hi} and Th17 subsets, IL-22^{+} IL-17A^{-} p=0.0312, IL-22^{-} IL-17a^{+} p=0.0312. Data for **d**, **f**, show mean ± SD, and min/max/median for **g**. p-values (NS≥0.05, *p<0.05, **p<0.01, ***p<0.001, ****p<0.0001) by Mann-Whitney test in **d**, Friedman test with Dunn multiple comparisons test in **f**, Wilcoxon test in **g**.

Author Manuscript Author Manuscript Author Manuscript Author Manuscript

Author Manuscript Author Manuscript Author Manuscript Author Manuscript

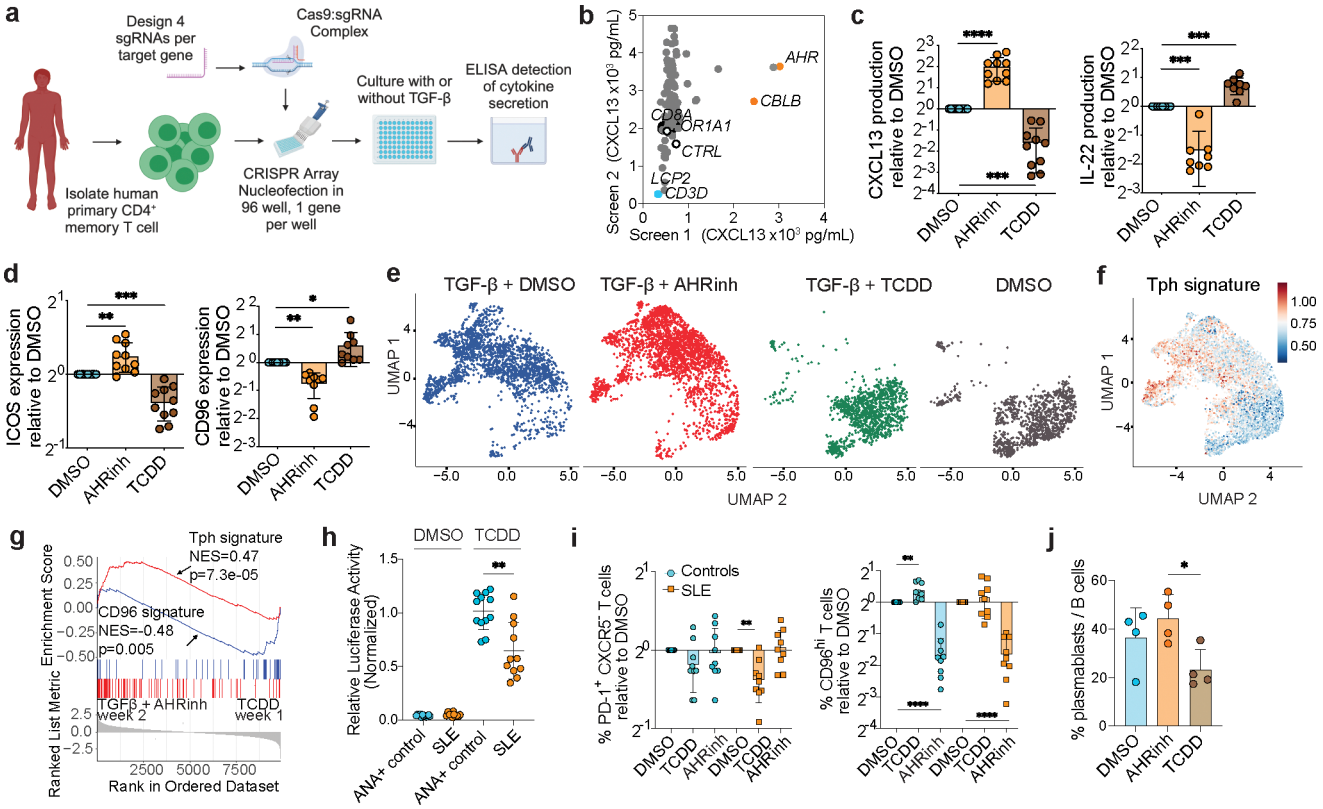

Figure 2. AHR controls a CXCL13-IL-22 differentiation axis in human T cells.

a, Schematic of arrayed CRISPR screen. **b**, CXCL13 quantification by ELISA from cells in CRISPR screen with TGF-β. Results from 2 independent experiments using different donors. **c**, ELISA quantification of cytokines, normalized to DMSO condition, from total CD4$^+$ T cells stimulated as indicated with TGF-β (n=10). For AHRinh and TCDD, respectively, p=1.44e-6 and 1.55e-4 for CXCL13, and p=1.33e-4 and 2.76e-4 for IL-22. **d**, Flow cytometry quantification of ICOS and CD96 on memory CD4$^+$ T cells, normalized to DMSO condition (n=8). For AHRinh and TCDD compared to DMSO, respectively, p=0.0052 and 0.0004 for ICOS, p=0.0020 and 0.018 for CD96. **e**, UMAPs of scRNA-seq data of memory CD4$^+$ T cells stimulated under indicated conditions for 2 weeks. **f**, UMAP as in **e** coloured by enrichment of Tph gene signature. **g**, GSEA plot of Tph gene signature enrichment (red) and CD96^{hi} gene signature enrichment (blue) in cells treated with TGF-β+AHRinh for 2 weeks versus TCDD without TGF-β for 1 week. **h**, AHR reporter activity in indicated conditions with serum from SLE patients (n=11) or anti-nuclear antibody (ANA)+ controls (n=12), p=2.80e-3. **i**, Flow cytometry quantification of indicated cell populations, normalized to DMSO condition, in T cells from PBMC of SLE or controls (n=9 each). Comparisons of AHR agonist/inhibitor to DMSO for SLE or control. For PD-1$^+$CXCR5$^-$ p=0.0022. For CD96^{hi}, from left to right, p=0.0041, 2.2e-5, 7.9e-5. **j**, Quantification of CD38^{hi} CD27$^+$ plasmablasts in co-cultures of B cells with Tfh cells pretreated as indicated (n=4 donors), p=0.021. **c, d, h-j** show mean ± SD. p-values (*p<0.05, **p<0.01, ***p<0.001, ****p<0.0001) by ratio paired t-test in **c**,**d**,**i** and **j**, Mann-Whitney test for **h**. TCDD = AHR agonist; AHRinh = AHR inhibitor CH-223191.

Author Manuscript Author Manuscript Author Manuscript Author Manuscript

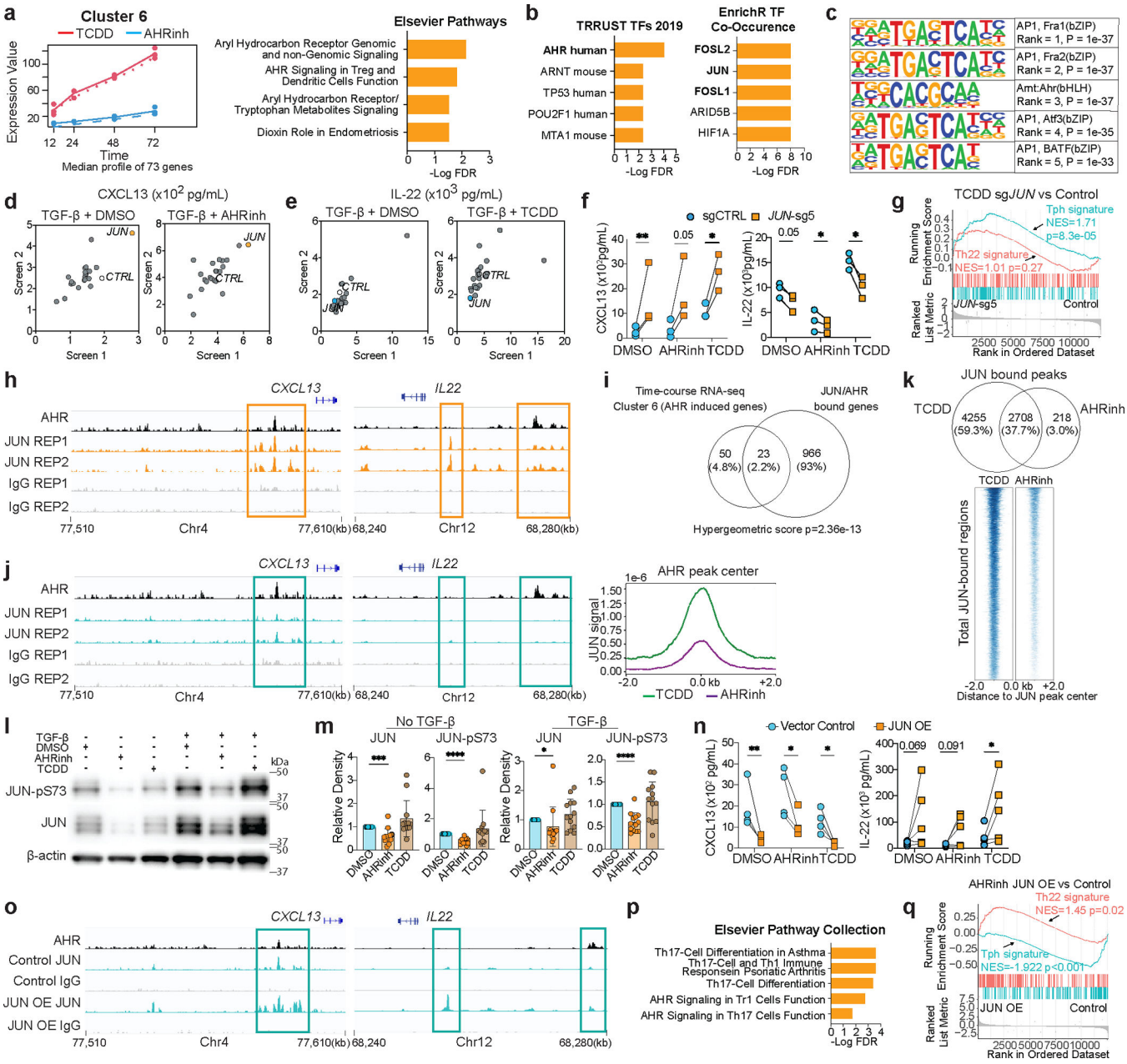

Figure 3. AHR coordinates with JUN to promote Th22 over Tph/Tfh phenotypes.

a, AHR-induced gene cluster identified by maSigPro and pathway enrichment. **b**, Enrichment of transcription factors and co-occurrence from **a**. **c**, AHR CUT&RUN motif analysis. **d**,**e**, ELISA quantification of CXCL13 (**d**) and IL-22 (**e**) from AP-1-targeted arrayed CRISPR screen of T cells (n=2, biological). **f**, CXCL13 (n=3) and IL-22 (n=3) production by T cells after JUN CRISPR, from left to right p=0.00979, 0.0528, 0.0108, 0.0517, 0.0226, 0.045. **g**, GSEA of Th22 (p=0.27) and Tph (p=8.3e-05) signatures in T cells with *JUN*-sg5 or control. **h**, Representative JUN binding peaks and AHR binding peaks in T cells treated with TCDD. **i**, Venn diagram of JUN and AHR co-bound peak-associated genes that overlap with cluster 6 (AHR-induced) genes from **3a**. **j**, Representative JUN

Author Manuscript Author Manuscript Author Manuscript Author Manuscript

binding peaks in AHRinh-treated T cells (left) and overall JUN binding signal (right) at AHR peaks in T cells treated with TCDD or AHRinh. **k**, Venn diagram and heatmap of JUN bound peaks in T cells treated with TCDD and AHRinh. **l**, Western blot of JUN and JUN-pS73 in T cells stimulated as indicated. **m**, Densitometry quantification of Western blot as in **g,** normalized to DMSO condition (n=13), from left to right p=0.0010, 3.1e-5, 0.0265, 6.6e-5. **n**, ELISA quantification of indicated cytokines in JUN-overexpressing (JUN OE) or control-transduced T cells, stimulated in TGF-β as indicated (n=4). From left to right p=0.00343, 0.0153, 0.0312, 0.069, 0.091, 0.0391. **o**, JUN binding peaks of AHRinh-treated T cells expressing empty vector or JUN overexpression vector (JUN OE) at *CXCL13* and *IL22* loci. **p**, Pathway enrichment analysis of genes associated with enriched peaks in JUN OE T cells. **q**, GSEA of Th22 (p=0.02) and Tph (p<0.001) gene signature enrichment in JUN OE and control T cells treated with AHRinh. **h** shows mean ± S.D. p-values obtained by ratio paired t-test for **f, m, n**. T cells = memory $CD4^+$ T cells.

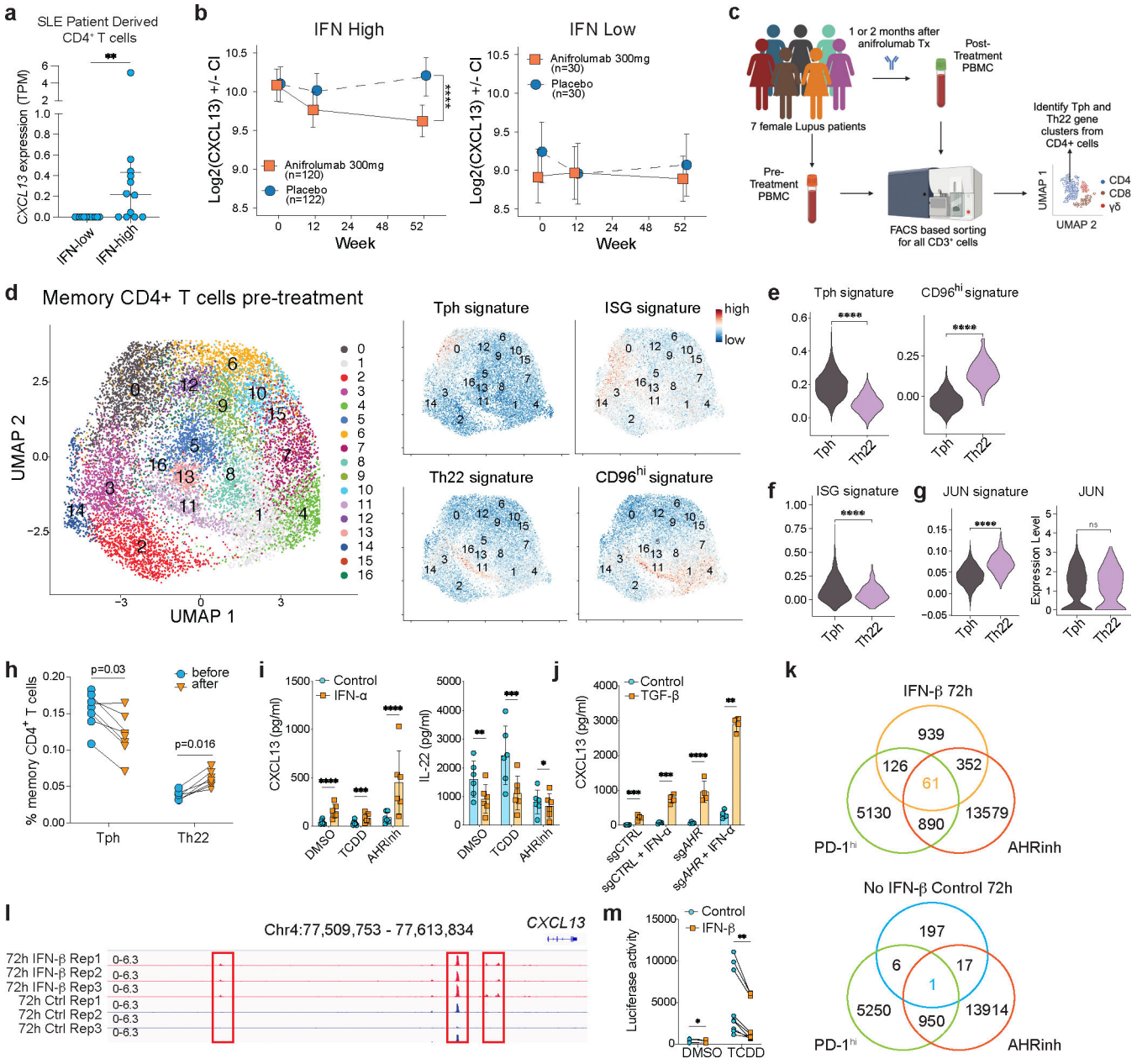

Figure 4. Increased IFN in SLE patients promotes Tph cell differentiation and inhibits AHR.

a, *CXCL13* in CD4$^+$ T cells from ISG^{hi} and ISG^{low} SLE patients (n=12, p=0.0013). **b**, Serum CXCL13 in SLE patients treated with anifrolumab or placebo, stratified by IFN signature level. Sample size as indicated. Error bars indicate 95% confidence intervals. For IFN High p=2.67e-07 by mixed effect model for 1 year trajectory. **c**, Schematic of scRNA-seq data generation. **d**, UMAP clustering of memory CD4$^+$ T cells from lupus patients pre-anifrolumab and feature plots for indicated gene signatures. **e**, Violin plots of expression of indicated signatures (from **1e**) in Tph and Th22 clusters. p<2.2e-16 for Tph, p<2.2e-16 for CD96^{hi}. **f**, Violin plots of ISG signature (p=4.57e-8), JUN transcriptional signature (p<2.2e-16) and JUN mRNA expression (p=0.81) in Tph and Th22 clusters from **d**. **h**, Tph and Th22 cluster proportions among memory CD4$^+$ T cells before and after anifrolumab. p=

Author Manuscript Author Manuscript Author Manuscript Author Manuscript

Author Manuscript Author Manuscript Author Manuscript Author Manuscript

0.03 for Tph, 0.016 for Th22. **i**, Cytokine quantification by ELISA from memory $CD4^+$ T cells stimulated as indicated (n=6). From left to right, p-value for CXCL13: 8.5e-5, 4.05e-4, 2.9e-5; for IL-22: 2.35e-3, 8.76e-4, 0.0338. **j**, ELISA for CXCL13 in total $CD4^+$ T cells nucleofected with sg*AHR* or control CRISPR guides, stimulated under indicated conditions (n=4). p-value from left to right: 5.17e-4, 2.8e-4, 7.1e-5, 1.35e-3. **k**, Venn diagram of overlapped DAR regions in IFN-β-treated $CD4^+$ T cells (left) or control (right) with SF PD-1^{hi} and AHRinh treated $CD4^+$ T cells. **l**, Accessible regions near *CXCL13* locus in $CD4^+$ T cells treated with IFN-β or control. **m**, AHR reporter activity in cells stimulated as indicated with or without IFN-β pre-treatment (3 experiments with 2–4 replicates each, total n=9, left to right p=0.0117, 0.00391). **a**, **i**, and **j** show mean ± S.D. p-value (*p<0.05, **p<0.01, ***p<0.001) by Mann-Whitney in **a**, linear mixed model in **e**, **f**, **g** and **m**, paired t-test in **h**, ratio paired t-test in **i** and **j**.

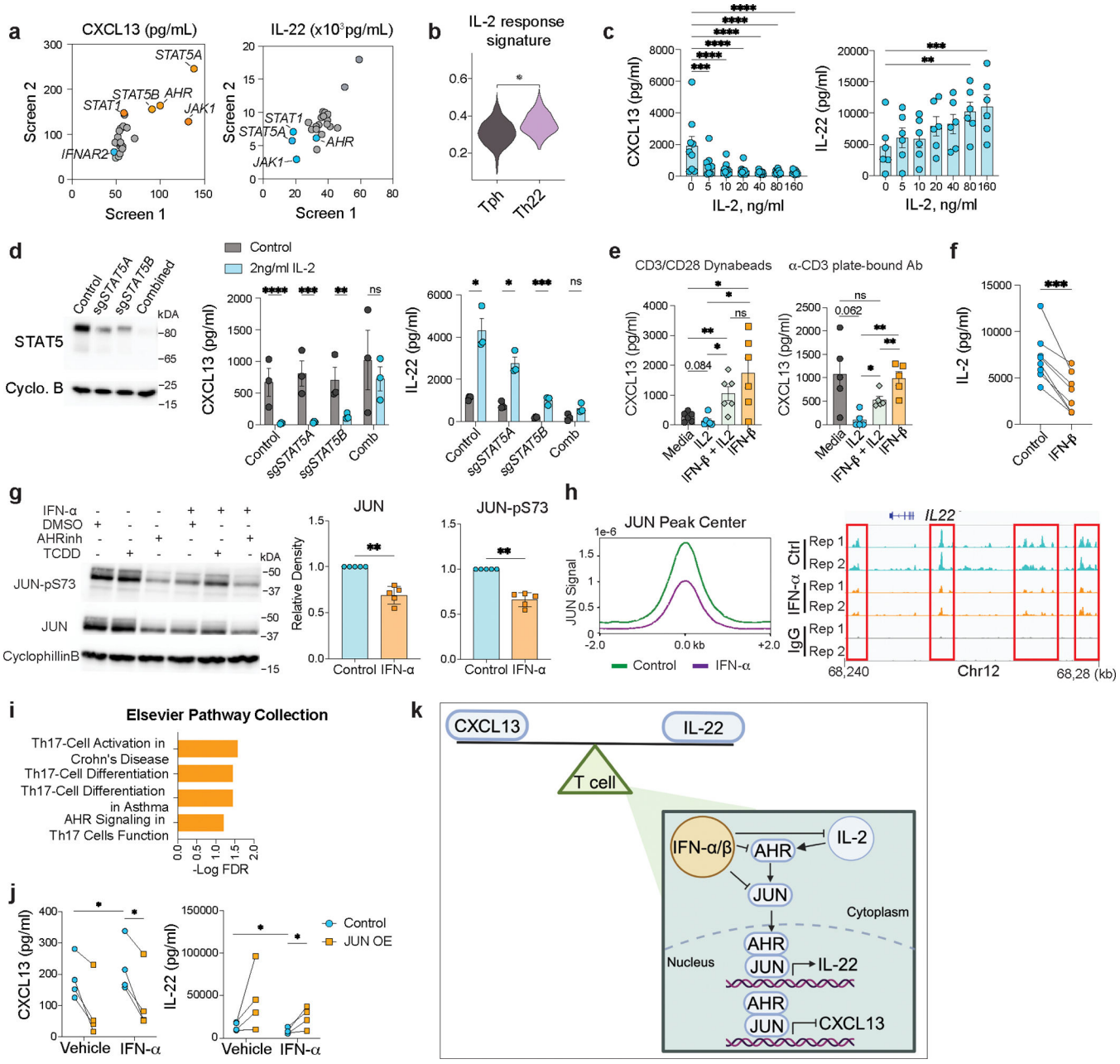

Figure 5. IFN opposes IL-2 and JUN to promote CXCL13^{+} Tph cells.

a, Cytokines by ELISA from cells from IFN-targeted arrayed CRISPR screen. Results of 2 independent experiments using different donors. **b**, IL-2-induced gene signature in Tph and Th22 clusters. p=0.0175. **c**, Cytokines by ELISA from memory CD4^{+} T cells stimulated with plate-bound anti-CD3 antibody and IL-2 at indicated concentrations. From left to right, p-values for CXCL13: 9.45e-4, 4.34e-5, 1.34e-5, 3.05e-6, 4.30e-6, 4.24e-6 and for IL-22: 2.21e-3, 4.51e-4. **d**, Western blot for STAT5 and ELISA for cytokines from memory CD4^{+} T cells nucleofected with sg*STAT5A*, sg*STAT5B*, both (combined) or control CRISPR guides, stimulated as indicated (n=3). Comparison of IL-2 effect within each CRISPR condition. p-values from left to right for CXCL13: 4.16e-5, 4.12e-4, 1.73e-3; IL-22: 1.94e-2, 2.53e-2,

Author Manuscript Author Manuscript Author Manuscript Author Manuscript

Author Manuscript Author Manuscript Author Manuscript Author Manuscript

6.06e-4. **e**, ELISA for CXCL13 from memory CD4+ T cells stimulated under indicated conditions. p-value from left to right for anti-CD3/CD28 (n=6): 5.52e-3, 1.70e-2, 1.08e-2, 2.40e-2; anti-CD3 antibody (n=5): 2.54e-2, 7.2e-3, 1.57e-2. **f**, ELISA for IL-2 from memory $CD4^+$ T cells stimulated with anti-CD3/CD28 as indicated (n=8), p=0.0008. **g**, Western blot for phosphoS73-JUN and JUN in memory $CD4^+$ T cells under indicated conditions and quantification normalized to control (n=5). JUN p=0.0044, JUN-pS73 p=0.0016. **h**, JUN binding signal at JUN peaks in memory $CD4^+$ T cells stimulated with or without IFN-α and representative JUN binding peaks at *IL22*. **i**, Pathway enrichment for annotated differentially bound peaks by JUN enriched in control versus IFN-α-treated conditions from **h**. **j**, ELISA for cytokines from memory $CD4^+$ T cells with JUN overexpression (JUN OE) or control with or without IFN-α (n=4). p-values from left to right for CXCL13: 0.011, 0.041; IL-22: 0.013, 0.033. **k**, Model of factors influencing Tph versus Th22 balance. **c**, **d**, **e**, **g** show mean ± S.E.M. p-value (*p<0.05, **p<0.01, ***p<0.001) by linear mixed model in **b**, 2-way ANOVA in **c**, ratio paired t-test in **d**, **e**, **f**, **g**, **j**.